*Geophys. J. Int.* (2003) **154,** 599–617

# Palaeomagnetic study of the El Quemado complex and Marifil formation, Patagonian Jurassic igneous province, Argentina

Maria P. Iglesia Llanos,[1]* Roberto Lanza,[2] Alberto C. Riccardi,[3] Silvana Geuna,[1] Marinella A. Laurenzi[4] and Raffaella Ruffini[5]†

[1]*Laboratorio de Paleomagnetismo 'Daniel Valencio', Departamento de Ciencias Geológicas, Universidad de Buenos Aires, Pabellón* 2, *Ciudad Universitaria,* 1428 *Buenos Aires, Argentina*
[2]*Dipartimento di Scienze della Terra, Università di Torino, Via Valperga Caluso* 35, 10125 *Torino, Italy*
[3]*Departamento Paleozoologia Invertebrados, Museo de La Plata,* 1900 *La Plata, Argentina*
[4]*Istituto di Geoscienze e Georisorse, CNR, Area della Ricerca di Pisa, via G. Moruzzi* 1, 56124 *Pisa, Italy*
[5]*Dipartimento di Scienze Mineralogiche e Petrologiche, Università di Torino, Via Valperga Caluso* 35, 10125 *Torino, Italy*

Accepted 2002 December 6. Received 2002 December 6; in original form 2001 November 15

## SUMMARY

The upper Jurassic El Quemado Complex was sampled at 36 sites from five localities in the cordilleran foothills of southern Patagonia between Lago Argentino and Lago Posadas–Sierra Colorada, and the middle Jurassic Marifil Formation at 12 sites in the Somuncurá Massif near Camarones. The main lithology was ignimbrite, with minor tuff and lava. Petrographical and SEM observation show that the El Quemado rocks suffered an intense, high-temperature alteration which resulted in transformation of most primary Ti-magnetite in pseudobrookite, rutile and minor Ti-haematite and Fe hydrated oxides. A similar, less pronounced alteration occurred in the Marifil rocks. $^{40}Ar/^{39}Ar$ dating of El Quemado was possible for one sample from Sierra Colorada and yielded an age of 156.5 ± 1.9 Ma. Magnetic mineralogy measurements (isothermal remanence, hysteresis loop, Curie balance) show that the remanent magnetization is dominated by PSD low-Ti magnetite, often associated to a minor high-coercive mineral (haematite). Secondary magnetization components are usually absent or weak at El Quemado sites, strong at Marifil. They were completely erased by thermal and AF demagnetization and a characteristic remanence (ChRM) stable up to temperatures higher than 550°C or peak-field values of 100 mT was successfully isolated.

The virtual geomagnetic pole (VGP) from the Marifil Formation (83°S, 138°E) is in agreement with the literature data for Jurassic rocks from stable South America. The El Quemado VGPs fall in two groups. The localities to the north of latitude 48°S (Lago Posadas, Sierra Colorada) yield a VGP (81°S, 172°E) close to that of Marifil, whereas those south of latitude 49°S (Lago San Martín, Lago Argentino) show a highly elongated VGP distribution consistent with counter-clockwise block-rotation about vertical axes. These rotations were likely caused by thrust sheets which were rotating counter-clockwise at the same time they were advancing towards the foreland. The amount of rotation varies according to the location of the sampling sites in the thrust and fold belt.

**Key words**: Jurassic, palaeomagnetism, Patagonia, volcanic structure.

## 1 INTRODUCTION

Palaeomagnetic studies on the Jurassic rocks of Argentina began in the early 1970s (Valencio & Vilas 1970; Creer *et al.* 1972; Vilas 1974) and were mainly intended to contribute to the South America apparent polar wander (APW) path. It was then interpreted (Valencio *et al.* 1983; Oviedo & Vilas 1984) that APW had been small during the middle to late Mesozoic and the stable South America poles had remained in almost the same position close to the present geographic pole. This conclusion has been questioned by Iglesia Llanos (1997) and Vizán (1998), who on the grounds of both new and reassessed literature data propounded a small loop in the APW path between 200 and 175 Ma. Interpretation of the Jurassic part of the South America APW path is hampered by the fact that many palaeomagnetic data derive from magmatic

*Now at: Institut für Allg. und Angew. Geophysik, Ludwig-Maximilians-Universität München, Theresienstrasse 41, D-80333 München, Germany. E-mail: paula@geophysik.uni-muenchen.de
†Deceased 2002 October 20.

rocks, whose age and tectonic setting are often poorly constrained. Moreover, possible intracontinental movements (Geuna *et al.* 2000) may introduce further uncertainties. Several recent papers (Vizán 1998; Geuna *et al.* 2000; Iglesia Llanos & Riccardi 2000) have investigated the Jurassic sedimentary sequences in northern and central Patagonia, whereas very few data are available for Jurassic rocks of southern Patagonia (Burns *et al.* 1980; Grunow *et al.* 1993; Roperch *et al.* 1997). More palaeomagnetic data from this region would be useful to a more detailed definition of the South America APW path and a better understanding of the geodynamic evolution of southernmost Andes.

This paper reports on a palaeomagnetic study made by a joint team from the Buenos Aires, La Plata and Torino universities and focussed on the upper Jurassic-lower Cretaceous El Quemado volcanic complex. A total of 36 sites was sampled at five localities in the Cordillera Patagonica foothills between Lago Argentino and Lago Posadas–Sierra Colorada. The study was supplemented by sampling twelve sites in the middle Jurassic Marifil Formation in extra-Andean Patagonia near Camarones.

## 2 GEOLOGICAL SETTING AND SAMPLING

Patagonia can be divided into two main tectonic regions: Andean Cordillera and extra-Andean. The Patagonian Andean Cordillera is along the Argentine-Chilean boundary on the western active margin of the South America plate and its evolution is related to subduction of the Nazca and Antarctic plates. The extra-Andean Patagonia is part of a passive continental margin, where two structurally stable areas have been recognized, the Somuncurá Massif to the north and the Deseado Massif to the south. The San Jorge Basin is located between these two massifs and the Magallanes basin to the south-southeast of the Deseado Massif.

Jurassic volcanic rocks are widespread in the whole region. In extra-Andean Patagonia they are represented by the Marifil (MF) and Lonco Trapial (LT) Formations, respectively in the east-southeast and west-southwest of the Somuncurá Massif, and the Chon Aike Formation (CA) in the Deseado Massif (Fig. 1). In the Patagonian Cordillera they form the El Quemado Complex (EQ) and its Chilean equivalent, the Ibañez Formation. General composition changes from mesosilicic-acidic in the cordillera to mainly rhyolitic in the extra-Andean regions. Recent $^{40}Ar/^{39}Ar$ and U/Pb investigations (Alric *et al.* 1996; Féraud *et al.* 1999; Pankhurst *et al.* 2000) show that the magmatic activity spanned about 40 Myr. It began in the northern part of the area in early Jurassic times and migrated south-westwards up to the late Jurassic–early Cretaceous. Pankhurst *et al.* (2000) identified three peaks in volcanic activity and proposed their correspondence with the three main volcanic units of Patagonia: 188–178 Ma (Marifil Formation), 172–162 Ma (Chon Aike Formation), 157–153 Ma (El Quemado Complex). This migration has been related to propagation of extensional features due to the break-up of Gondwana and change in the geometry of the subduction zone to the west, along the Pacific margin of the continent (Alric *et al.* 1996; Féraud *et al.* 1999; Pankhurst *et al.* 2000).

### 2.1 El Quemado Complex

In the Patagonian Cordillera, volcanic rocks crop out over a large area as a narrow, almost continuous belt along the Patagonian-Fueguian Andes, whereas to the east they are restricted to the subsurface of the Austral Basin. The El Quemado Complex mostly consists of rhyolitic and dacitic ignimbrites with minor lava flows and volcaniclastic rocks, which in some areas lie on a basal breccia or conglomerate. Andesite composition increases north of latitude 47°S and south of 49°S (Ramos *et al.* 1982; Gust *et al.* 1985). These rocks were formed in a volcanic arc that marked the initiation of subduction of the Proto-Pacific plate in the argentinian Patagonia (Bertrand *et al.* 1999; Féraud *et al.* 1999; Panza & Haller 2002; Ramos 2002). During this time, an extensional state of stress prevailed, so that the volcanic rocks of El Quemado appear in local depocentres associated with thick, coarse-grained sedimentites between normal faults. The El Quemado Complex usually overlies Palaeozoic sedimentary and metamorphic rocks and at Lago Argentino the upper levels are interbedded with marine rocks of the Zapata Formation, which have yielded a late Jurassic–early Cretaceous invertebrate fauna (Riccardi *et al.* 1992). Dating by U/Pb (on zircons) and $^{40}Ar/^{39}Ar$ (on K-feldespars grains) have given ages comprised between 153 and 155 Ma and 144 and 170 Ma, respectively (Féraud *et al.* 1999; Pankhurst *et al.* 2000). Most published K/Ar and Rb/Sr ages fall within the range of the $^{40}Ar/^{39}Ar$ ages (Nullo *et al.* 1978; Ramos 1979, 1981; Ramos *et al.* 1982; Pankhurst *et al.* 1993; Suárez & De la Cruz 1997; Suárez *et al.* 1997), spanning the Bathonian–Berriasian (Ogg 1995; Gradstein *et al.* 1995). Some anomalous younger ages may be due to resetting either by tectonic deformation (Halpern 1973) or during the successive emplacement stages of the Patagonian batholith (Pankhurst *et al.* 1993).

The tectonic features along the Patagonian Andes between Lago Argentino (50°S) and Lago Posadas–Pueyrredón (47°S) have been described by various authors (Nullo *et al.* 1978; Ramos 1981, 1982, 1989; Massabie 1990; Kraemer 1993; Giacosa *et al.* 1999; Kraemer *et al.* 2002). Basically, the region is characterized by north-south trending structural features of the Patagonian thrust and fold belt, which formed from late Cretaceous with two special pulses of deformation in the Eocene and Miocene (Ramos 1989; Kraemer 1994). The orogenic belt has been subdivided by Kraemer (1994) and Kraemer *et al.* (2002) in a western andean flank (towards the Pacific), an inner (magmatic arc or Patagonian Batholith and inner fold and thrust belt) and an eastern andean region (outer fold and thrust belt). In the inner andean region, deformation is maximum and affects mainly the basement of the basin (Palaeozoic and the Jurassic volcanics). In the outer fold and thrust belt on the other hand, there is a diminishing deformation towards the east and a north-south change in the structural style where deformation has an effect mainly in the basement (thick-skinned) north of 49°S, and in the sedimentary Cretaceous-Tertiary cover (thin-skinned) to the south of that latitude. The morphological and structural features of the Patagonian fold and thrust belt between 47° and 52°S vary considerably from north to south. One of the most noticeable aspects is that the inner part of the orogenic belt decreases in width from 150 km at 47°S to less than 50 km at 52°S; conversely, the outer part reaches its maximum width at the latitude of Lago Argentino (50°S). Such structural changes appear to be associated to transverse lineaments, which would have been active during the Jurassic–Cretaceous (Arbe 1988; Kraemer 1994; Kraemer *et al.* 2002) or older orogenies (Nullo *et al.* 1978; Ramos 1979, 1983). These lineaments coincide with that of the main lakes of the region: Pueyrredón, Belgrano, San Martín, Viedma and Argentino.

The cause of the changes in the structural style of segments are interpreted as their different response to Andean shortening, which in turn depends on the amount of stretching that segments underwent during the initial Jurassic rifting stage (Kraemer 1994). On the other hand, Ramos (1989) remarks the contemporaneity of events between the formation of structural features at these latitudes and the collision of segments of the Chile Ridge with the Patagonian Cordillera during

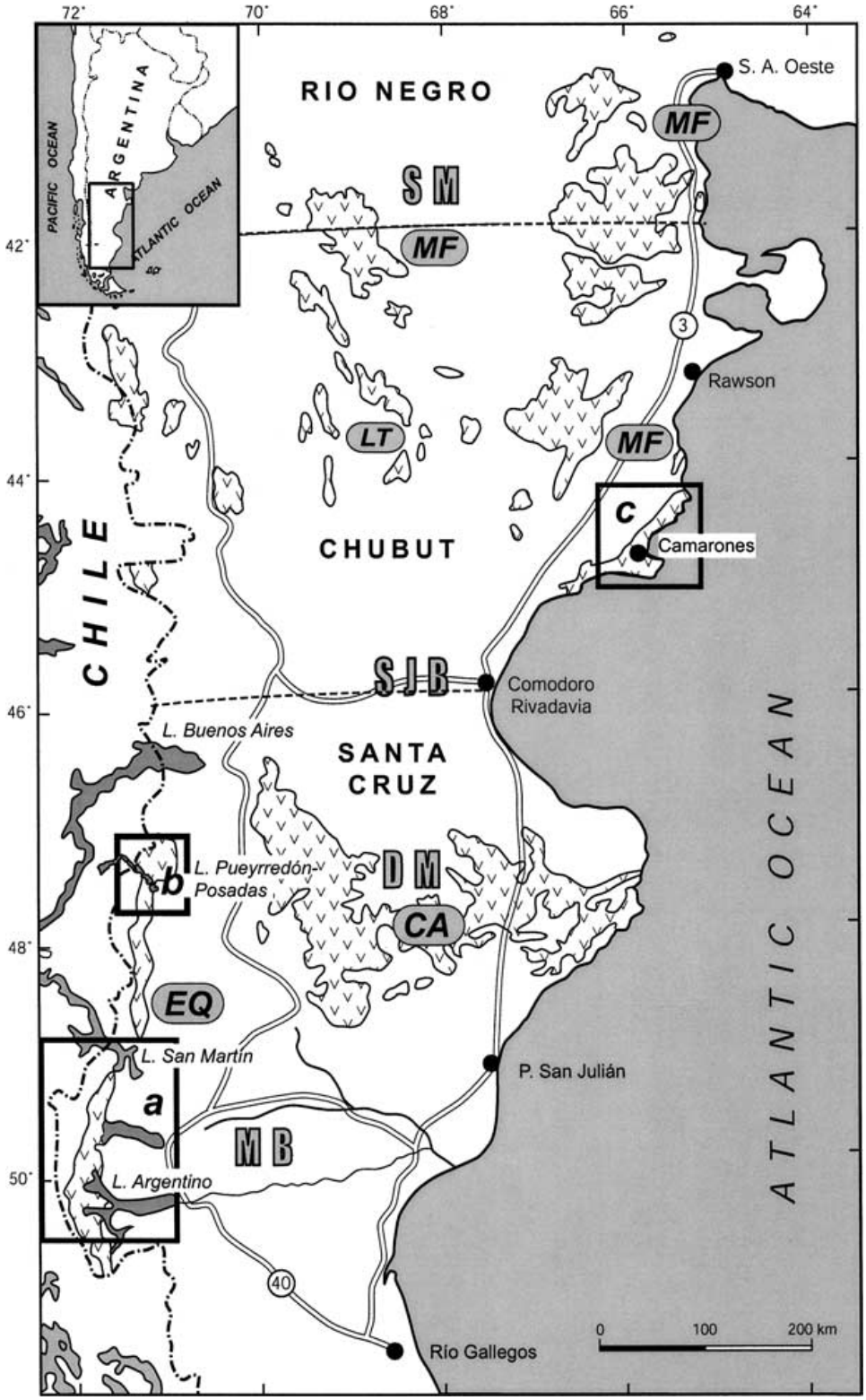


**Figure 1.** Sketch map of of the Jurassic volcanic province of Patagonia. LT = Lonco Trapial Group (centre of Chubut); MF = Marifil Formation (Río Negro and Chubut); CA = Chon Aike Formation (central-east Santa Cruz); EQ = El Quemado Complex (west of Santa Cruz). The palaeomagnetic sampling was carried out in EQ (a and b) and MF (c). SM = Somuncurá Massif; DM = Deseado Massif; SJB = San Jorge Basin; MB = Magallanes Basin.

periods of fast convergence. Compressive shortening in the fold and thrust belt has been estimated as 30 km at Lago Argentino, 22 km at Lago San Martín and 45 km at Lagos Posadas–Pueyrredón (Ramos 1988; Kraemer 1993).

Along with the N-NW trending folds and thrusts, basement and cover are affected by minor faults with vertical and lateral displacements, formed probably during the last stages of the deformation (Kraemer 1998). In the frontal monocline of the orogenic belt, geological evidences indicate left lateral displacements (Massabie 1990).

### 2.2 Marifil Formation

In extra-Andean Patagonia in the southeast of the Somuncurá Massif, the Jurassic volcanic rocks form the Marifil Formation, which mainly consists of flat lying, rhyolitic ignimbrite sheets with associated volcaniclastic deposits and lava flows. This formation has a total thickness up to 600–900 m. It unconformably overlies Precambrian and Palaeozoic rocks and is in turn overlain by Cretaceous continental sediments and Cenozoic marine and continental deposits. Rb/Sr and $^{40}Ar/^{39}Ar$ dating yields ages between 168.1 ± 2.1 and 187.4 ± 0.6 (Alric *et al.* 1996; Féraud *et al.* 1999; Rapela & Pankhurst 1993) which indicate that the Marifil Formation corresponds to the onset of Jurassic volcanism in Patagonia.

Most of the Marifil Formation is exposed to the east-northeast of the Gastre Fault zone, a major transcontinental shear zone trending NW–SE from the Andean Cordillera to Central Patagonia. The southeastern continuation of this fault zone is thought to cross the Atlantic coast immediately to the south of Bahía Camarones, based on the occurrence of vertical faults with a general strike N125°–130° and extension fractures and dykes striking N165° occurring in the Marifil rocks of this region (Rapela & Pankhurst 1992). According to these authors, a dextral displacement of about 500 km would have occurred along the Gastre Fault zone, during early to middle Jurassic times.

### 2.3 Sampling

Five localities were sampled in the El Quemado Complex (Fig. 2a and b) and one in the Marifil Formation (Fig. 2c). The sampling areas for El Quemado are located within the inner (Lago Argentino, Lago San Martín) and outer (Lago Posadas–Sierra Colorada) parts of the Patagonian fold and thrust belt. Each locality comprised six to twelve sampling sites arranged in pairs separated a few kilometres from each other. The two sites of each pair were cored in two distinct levels some tens of metres apart. The cores were oriented with both magnetic and solar compass, and magnetic declination was found to vary between 14°E (Lago Argentino) and 6°E (Bahía Camarones). At least one thin section was made for each site for petrographical and microprobe analyses. Some samples were also collected for $^{40}Ar/^{39}Ar$ dating.

*Lago Argentino (Estancia La Unión)*

The sampling was carried out in the El Quemado type locality, at the northwestern margin of Lago Argentino (Fig. 2a, U1-3), in the vicinity of Estancia La Unión. The Jurassic volcanics are the oldest rocks in the region and are unconformably overlied by Cretaceous marine sedimentites (Feruglio 1944, 1949; Furque 1973; Kraemer & Riccardi 1997). The whole series is folded in a broad, north-south striking anticline whose axis roughly coincides with the western slope of Cerro Hobler (Feruglio 1944). The regional dip is about 40°E with some minor second order folds. The sampling sites were located astride this anticline.

*Lago San Martín South (Estancia La Maipú)*

The sampled area is located on the southern coast of Lago San Martín in the southern and northeastern neighbourhood of Estancia La Maipú (Fig. 2a, M1-3). The geology here has been studied by Nullo (1978) and Nullo *et al.* (1978). Around Estancia La Maipú the rocks from El Quemado are widespread but the usually associated older and younger geological units are absent, so that the structural attitude of the volcanics is not straightforward. The structural outline of the area (Nullo *et al.* 1978) is a N-NE trending monoclinal which dips ≈30° E–SE.

*Lago San Martín North (Estancia Península Chacabuco)*

The sampled locality is situated north of Lago San Martín, immediately southwest of Bahía de la Lancha, along the road to the Estancia Península Chacabuco (Fig. 2a, CH1-3). The volcanic rocks of El Quemado unconformably overlie folded Palaeozoic turbidites (Bonarelli & Nágera 1921; Riccardi 1971). Regionally they form a broad anticline that covers a nucleus of Palaeozoic rocks quite well exposed on the western and eastern shores of Península Chacabuco and the eastern margin of Bahía de la Lancha. The regional dip of the volcanic rocks is 6° to 25° E-SE east of Bahía de la Lancha and about 10°S to the south of Península Chacabuco.

*Lago Posadas (Estancia El Furioso)–Sierra Colorada (Paso Roballos)*

Two areas were sampled in this region, one along the road which follows the northern shore of Lago Posadas (Fig. 2b, F1-6) and another in Sierra Colorada (Fig. 2b, R1-3), along the road from the town of Lago Posadas to Paso Roballos. The rocks of the El Quemado Complex are the oldest in this area and are unconformably overlain by some relicts of upper Jurassic sediments (Riggi 1957; Giacosa *et al.* 1999). The Sierra Colorada is affected by two major thrusts running north-south, i.e. the El Salitral and Sierra Colorada faults, as well as by minor faults oriented NW–SE/NE–SW. The first of the major faults constitutes the oriental boundary of the Sierra and marks the easternmost advance of the deformation north of the Pueyrredón lineament (Giacosa *et al.* 1999). At the sampling sites close to Lago Posadas the volcanic rocks dip gently towards the west, whereas at Sierra Colorada the attitude varies from site to site, reflecting local block tectonics.

#### *2.3.1 Bahía Camarones*

The Marifil rocks crop out along the coasts of Bahía Camarones (Fig. 2c). Immediately to the west, they are bounded by a NE–SW striking lineament and then covered by Neogene deposits (Camacho 1979; Lema *et al.* 2001). They mainly consist of strongly welded ignimbrites and rhyolitic to trachyandesitic lava flows. The sampling sites are located to the south and north of the town of Camarones, along the road to Cabo dos Bahías and Cabo Raso respectively. According to Lema *et al.* (2001) structural lineaments are rare and not clearly visible.

## 3 PETROGRAPHY AND GEOCHRONOLOGY

The petrography and geochemistry of the El Quemado and Marifil rocks have been thoroughly investigated in the literature (Gust *et al.* 1985; Sruoga 1989; Rapela & Pankhurst 1993; Pankhurst *et al.* 1998). The present paper only refers to the rocks sampled for the palaeomagnetic study and reports a brief description of the main petrographic and minerochemical features to characterize the magnetic

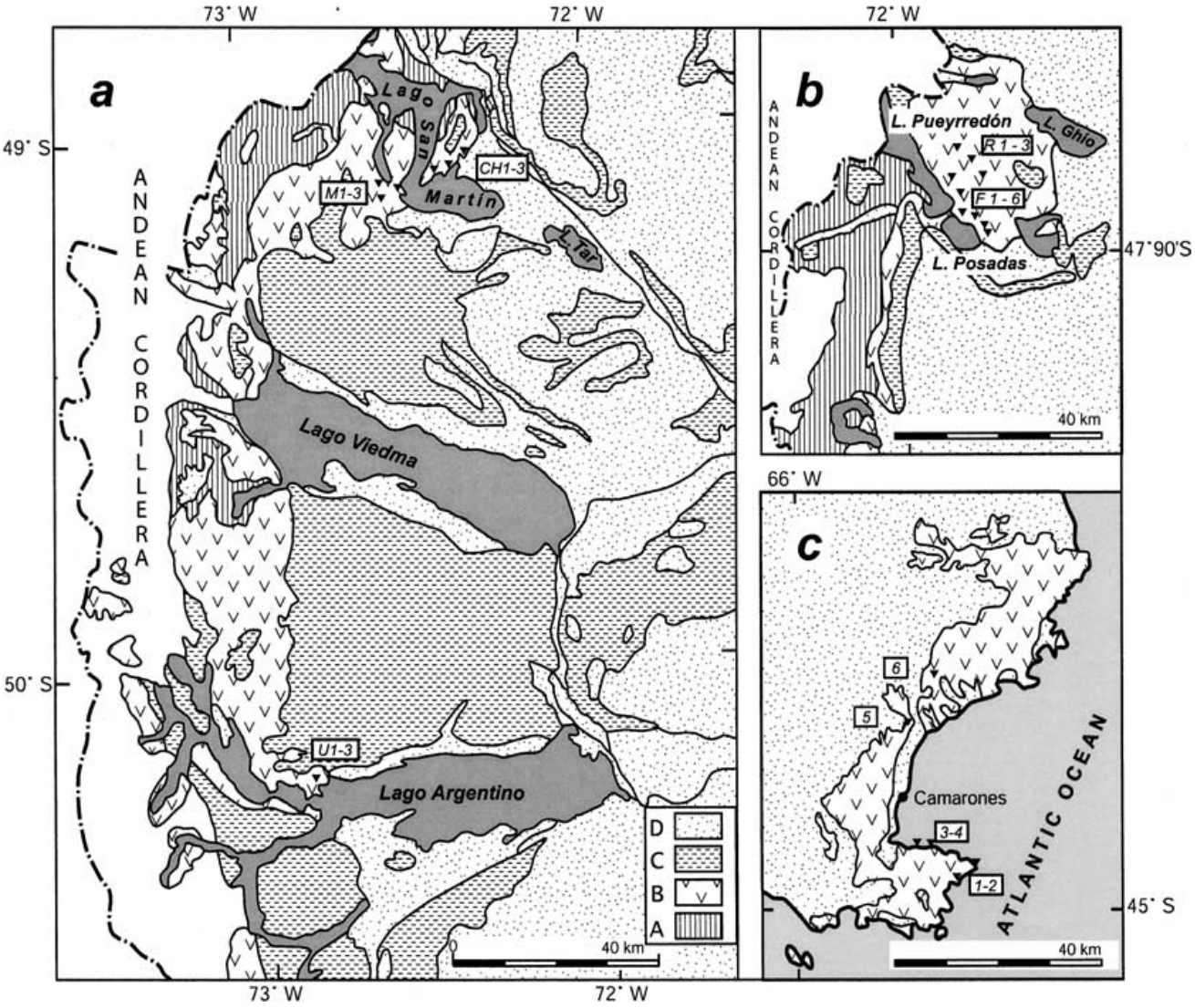


**Figure 2.** Geological sketch maps and sampling sites. El Quemado Complex: (a) localities San Martín North (sites *CH* = Estancia Península Chacabuco), San Martín South (*M* = Estancia La Maipú) and Lago Argentino (*U* = Estancia La Unión); (b) localities Sierra Colorada (*F* = Estancia El Furioso) and Lago Posadas (*R* = Sierra Colorada). Marifil Formation: (c) locality Camarones. Geological symbols: A: Palaeozoic basement; B: Jurassic volcanics; C: upper Jurassic-Cretaceous sediments; D: Cenozoic to Recent deposits.

minerals and analyse the effects of hydrothermal activity. Welded to densely welded ignimbrites are by far the predominat lithology. They have a phenodacitic to phenorhyolitic composition with a porphyricity index from 10 to 30 per cent. They show high content of glass shards, medium-sized crystals and lithic fragments, mainly cognate and minor xenoliths. Most of the groundmass sufferred various degree of devitrification and slight alteration. Pumiceous clasts and lithic fragments are common in the basal units. The main volcanic phases are quartz, plagioclase ($An_{48-42}Ab_{52-56}Or_{1-2}$), sanidine ($Or_{68-64}Ab_{26-30}An_2$), biotite and completely altered amphibole. Secondary alteration is widespread, particularly in the El Quemado rocks. The feldspars are generally altered to albite and psudemorphs of calcite and kaolinite. Original maphic phases are strongly affected by chloritization. The accessory minerals mainly consist of zircon, apatite and Fe–Ti oxides. Evidence from transmitted and reflected light microscopical observations suggests that Ti-magnetite and ilmenite were the primary oxides, the latter being more common in the ignimbrites from El Quemado. Besides small phenocrysts, their occurrence as inclusions in the other phenocrysts points to early crystallization (Carmichael 1967). The size typically ranges between 10 and 400 $\mu$m and the habit varies from equant or elongate to strongly xenomorphic with a red-yellow alteration rim. Magnetite and ilmenite were affected by strong deuteric oxidation that resulted in the formation of Ti-phases and Ti–Fe hydrated phases.

### 3.1 EDS microanalysis of Fe–Ti oxides

Detailed SEM observations and EDS microanalyses were carried out on Fe–Ti oxides grains from representative specimens of each site. Minerochemical analyses were done using a scanning electron microscope S360 Cambridge equipped with an energy dispersion spectrometer QX2000 of Link Analytical.

In the El Quemado rocks, primary Ti-magnetite and ilmenite are replaced by pseudomorphic oxidation products. The degree of

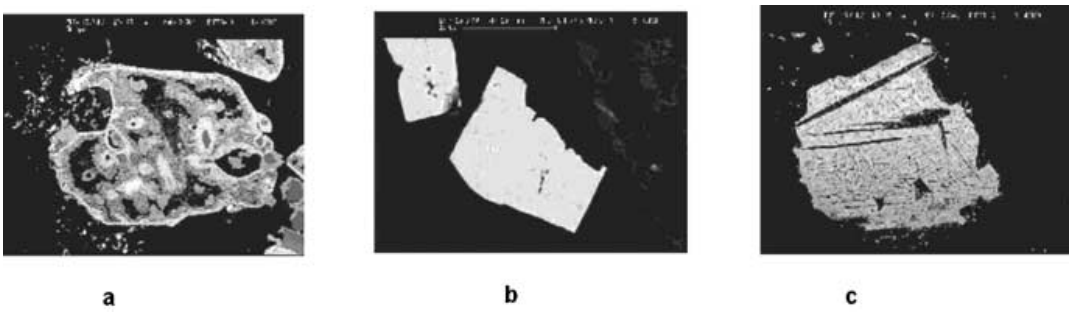


**Figure 3.** Backscattered electron images of Fe–Ti oxides. (a) Magnetite completely affected by oxidation (El Quemado, rhyolitic tuff). The bright border is haematite, the darker portion Fe–Ti hydrated oxides, the brigth homogeneous portion pseudo-brookite or rutile. (b) Completely pseudomorphed crystal from primary Ti-magnetite (El Quemado, dacite). The fine white lamellae are Ti-haematite. (c) Euhedral grain of Ti-magnetite (brighter) showing exsolved lamellae of ilmenite (darker) (Marifil Formation, trachi-rhyolite).

oxidation, and thus the oxidation products, varies in the samples from different sites and is probably related to the different ignimbrite structures, which in turn depend on the cooling rate (Cas & Wright 1987; Streck & Grunder 1995). In general, the coarse Ti-magnetite crystals underwent a first stage of oxidation exsolution with development of ilmenite lamellae. This oxidation occurred at high oxigen fugacity and temperature above 600°C (Haggerty 1976). A second stage of more intense oxidation resulted in the replacement of the lamellae of ilmenite and magnetite by deuteric pseudomorphic oxidation assemblages. They consist of pseudobrookite, rutile and Fe hydrated oxides developed along the original {111} planes of the exsolved ilmenite lamellae (Fig. 3a). Primary ilmenite is completely transformed in pseudobrookite, rutile and rare areas of Ti-haematite (Fig. 3b). In some samples from El Quemado, migration of Ti from the primary oxides is documented by widespread occurrence of rutile filling in cracks and voids. The mineralogical features of the oxidation products suggest that they formed at temperatures between 700 and 600°C (Haggerty & Lindsley 1970). In the Marifil rocks, most of primary Ti-magnetite shows the tick original exsolution lamellae of ilmenite completely oxidized to pseudobrookite and Ti-haematite. Alteration of Fe–Ti oxides, however, is less pronounced than in El Quemado and a well preserved, low-Ti magnetite (Ti $\approx$ 0.08 p.f.u.) is common. In some rocks, subhedral grains of magnetite with exsolved lamellae of ilmenite suggest that a primary Ti-magnetite with higher Ti content was also present (Fig. 3c).

### 3.2 Geochronology

Samples from the El Quemado rocks were collected for $^{40}Ar/^{39}Ar$ dating at many palaeomagnetic sites, but proved too altered to be successfully analysed. The only exception was a dacitic ignimbrite from Sierra Colorada (site R2), where alteration of plagioclase progresses in a non uniform way, depending on the zoning pattern of the mineral (Delvigne 1998). The alteration is in fact restricted to the more calcium-rich parts of the crystal (the cores), whereas the more sodium-rich zones (the rims) remain clear and free of any alteration. Biotite transformed to chlorite and few altered sanidines were also present in the sample. Analyses were performed as in-situ $^{40}Ar/^{39}Ar$ laser spot fusions on polished section (see Appendix).

Almost all analyses are from the outer rims of feldspars, mainly plagioclase with andesinic composition, but two from the groundmass. A cumulative probability plot of all analysed points shows a minor cluster around 120–130 Ma and a major one at 145–160 Ma. This spreading may reflect both the alteration of the rock and the tectonic history of the region. No relationships were observed between K/Ca ratio (0.06 $\div$ 8.5) and per cent $^{40}Ar_{rad}$ towards apparent ages. Inverse isochron diagrams were employed to treat analytical data, and K/Ca ratios (derived from $^{39}Ar/^{37}Ar$ ratios) were used to select points. EDS data on plagioclase display a K/Ca ratio from 0.02 to 0.07; few chronologic analyses have K/Ca $<$ 0.1. They are characterized by high scatter on ages (92 to 162 Ma), high errors and low radiogenic $^{40}Ar$ yields. Few points have K/Ca higher than 1: they are representative of ground mass and, likely, of relics of sanidine, with ages varying from 120 to 160 Ma. Neither this last group nor the previous one evidences an acceptable isochron. Half of the analysed points have K/Ca ratios between 0.1 and 1, and a narrow age interval (136 to 160 Ma); most of them identify an isochron of 156.5 $\pm$ 1.9 Ma ($1\sigma$) with a MSWD = 0.9 (Fig. 4). Some contribution of the groundmass is probable for all analysed points, due also to its better coupling with the IR laser beam, but there are not evidences that the calculated isochron is a mixing line.

The obtained age of 156.5 $\pm$ 1.9 Ma falls within the range of chronologic data for El Quemado. It is close to the U/Pb age of 154.1 $\pm$ 1.5 Ma from the same region of Sierra Colorada (Pankhurst *et al.* 2000) and somewhat older than the $^{40}Ar/^{39}Ar$ ages by Féraud *et al.* (1999), 147.1 $\pm$ 0.5 and 144.2 $\pm$ 0.4 Ma.

## 4 ROCK MAGNETISM

A total of about 330 and 100 specimens were analysed from the El Quemado Complex and Marifil Formation, respectively. They were measured in the Buenos Aires, Torino and Utrecht laboratories, using a KLY-2 or KLY-3 kappabridge to measure susceptibility and a JR-5 spinner or a 2G criogenic magnetometre to measure remanence. Procedures were basically the same in the three laboratories. In addition, the Curie balance (Mullender *et al.* 1993) and MicroMag-2900 were also used in Utrecht to investigate the magnetic mineralogy.

### 4.1 Magnetic mineralogy

Isothermal remanence (IRM) acquisition, back-field measurements and thermal demagnetization of a multicomponent IRM according to Lowrie (1990) were first carried out on at least one specimen per site. The results showed that the magnetic properties vary little within the rocks of each volcanic group and are not related to the various lithologies. MicroMag and Curie balance measurements were therefore performed on a reduced number of representative specimens.

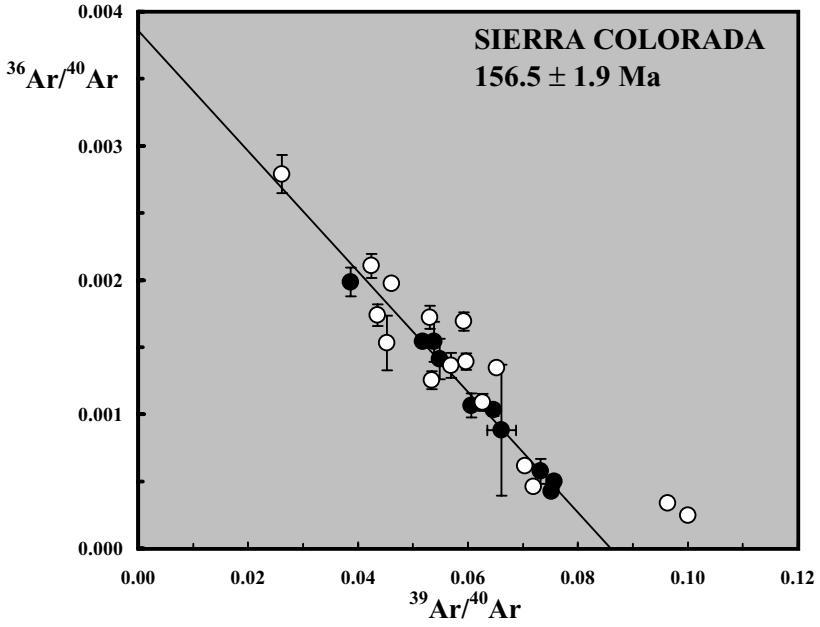


**Figure 4.** $^{36}Ar/^{40}Ar$–$^{39}Ar/^{40}Ar$ inverse isochron diagram. Reported age has been calculated from selected points (solid circles). Error bar = $\pm 1\sigma$.

*4.1.1 El Quemado Complex*

At most sites more than 95 per cent of the IRM saturation is reached at a field of 0.2 T (Fig. 5a), and the low-, intermediate- and high-coercivity IRM components are completely removed below 600°C (Fig. 6a). Hysteresis loops typically show complete saturation between 0.2 and 0.7 T and depict a pot-belly geometry (Fig. 7a) indicative of Ti-magnetite. The ratio of saturation remanence to saturation magnetization ($M_r/M_s$) ranges between 0.20 and 0.28 and that of coercivity of remanence to coercive force ($H_{cr}/H_c$) between 2.0 and 3.0, showing very consistent $H_{cr}$ values of 48 ± 5 mT. These samples fall (Fig. 8) in the pseudo single-domain (PSD) field of the Day plot (Day *et al.* 1977). Some specimens require a larger saturation field (>1 T), show higher $H_c$ and $H_{cr}$ values and their hysteresis loop is characterized by a wasp-waist geometry (Fig. 7b), due to the occurrence of a high coercive mineral, most likely haematite.

Curie balance measurements were performed on powders and yield two sets of Curie temperatures (Fig. 9), one indicative of low-Ti magnetite ($550 < T_c < 580$°C), the other of haematite/maghemite ($620 < T_c < 670$°C). The lower set is found in all measured samples, whereas the higher set is only observed in the rocks whose hysteresis properties show the occurrence of a high coercive mineral.

The results from IRM analyses, hysteresis loops and Curie balance thermomagnetic curves show that low-Ti magnetite in the PSD state is the more common ferromagnetic mineral, often associated with minor haematite and probably, maghemite. Widespread occurrence of haematite is restricted to four sites (Maipú 3, Chacabuco 1, Furioso1 and 6) where IRM saturation is only approached at the maximum available field of 1.6 T (Fig. 5b) and the IRM intermediate- and high-coercivity components withstand temperatures up to about 650°C (Fig. 6b). In particular, the site Furioso 1 yields the highest $H_c$ and $H_{cr}$ values, 90 and 370 mT respectively (Fig. 7b), and a Curie temperature of 650–660°C.

The magnetite grains reasonably correspond to the small, opaque grains embedded within the ignimbrites' glassy groundmass which are observed in high-magnification SEM images. Their size in the range 1 to 10 $\mu$m, however, is below the EDS resolution limit and direct analysis was thus not feasible. Occurrence of such grains both within the glassy groundmass and as the result of multiple division of large crystals is common in lavas and ignimbrites (Haggerty 1976; Xu *et al.* 1997; Zhou *et al.* 2000).

*4.1.2 Marifil Formation*

The IRM experiments show saturation fields of 0.15 to 0.2 *T* (Fig. 5c) and the IRM thermal demagnetization show a strong decrease of the low-coercivity component in the range $300°C < T < 400°C$ (Fig. 6c), coupled with a similar decrease of magnetic susceptibility. All three components are then usually removed between 560 and 570°C. The hysteresis loops depict both pot-belly and wasp-waist geometries (Fig. 7c). The first yields $M_r/M_s$ ratios around 0.16 and $H_c$ values between 10 and 12 mT. These features are indicative of Ti-magnetite, which is shown by the Day plot to occur in the PSD state (Fig. 8). The wasp-waist geometry on the other hand, has higher $H_c$ values, pointing to a higher coercive mineral such as haematite.

The thermomagnetic curves from the Curie balance measurements yield three sets of Curie temperatures, i.e. $T_c \approx 350$°C, $550 < T_c < 580$°C, $630 < T_c < 670$°C (Fig. 9). Occurrence of low Curie temperatures in rocks from Bahía Camarones region has already been reported by Creer *et al.* (1972). No evidence for pyrrhotite is found in our samples and EDS microanalyses suggest that the lowest $T_c$ set correspond to a Ti-rich magnetite. The intermediate and highest sets are indicative of low-Ti magnetite and haematite/maghemite. The magnetic mineralogy of the Marifil Formation, in conclusion, is similar to that of El Quemado Complex. The main differences are a less pronounced alteration and the occurrence in some rocks of two compositionally different Ti-magnetites.

### 4.2 Magnetic remanence

*4.2.1 El Quemado Complex*

The order of magnitude of the natural remanent magnetization (NRM) intensity varies in the range $10^{-4}$ to $10^{-1}$ A m$^{-1}$ (Table 1)

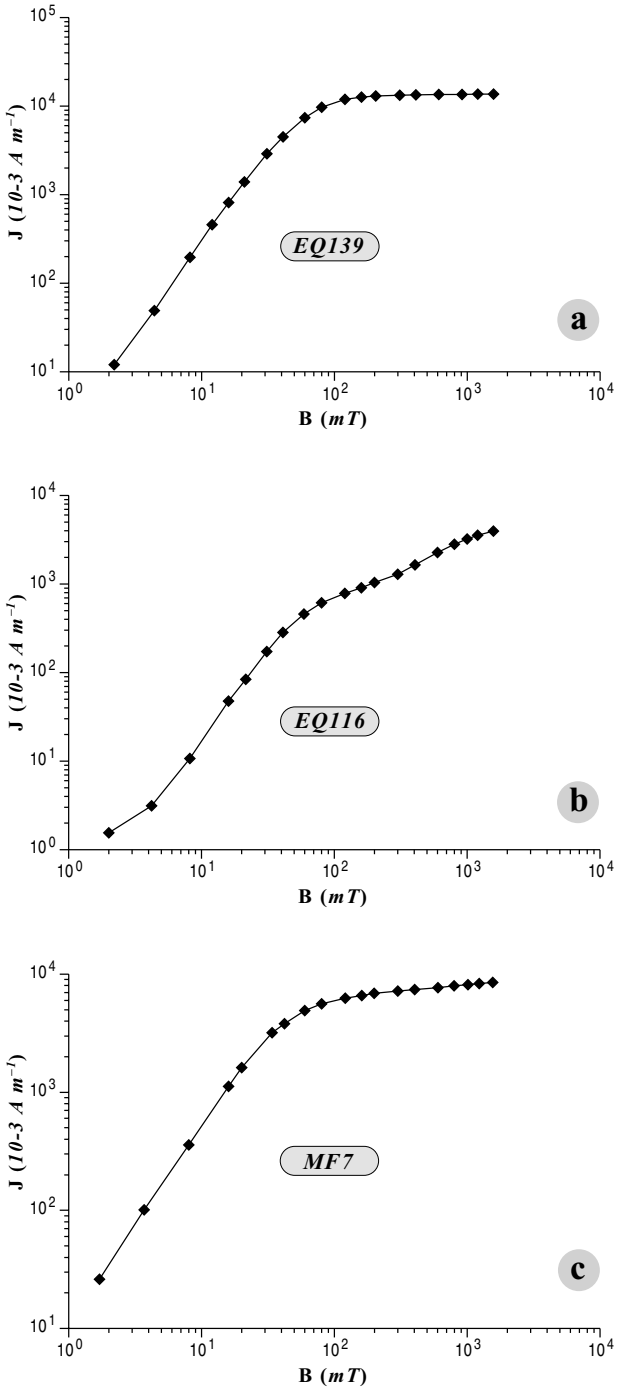


**Figure 5.** IRM acquisition curves for samples from the El Quemado Complex (a: site F3b; b: site F1b) and Marifil Formation (c: site Caleta Sara 4b). El Quemado shows generally (a) IRM saturation fields of 0.2 T and in a few sites (b) fields greater than 1.6 T. In Marifil, (c) IRM saturation fields are mainly between 0.15–0.2 T.

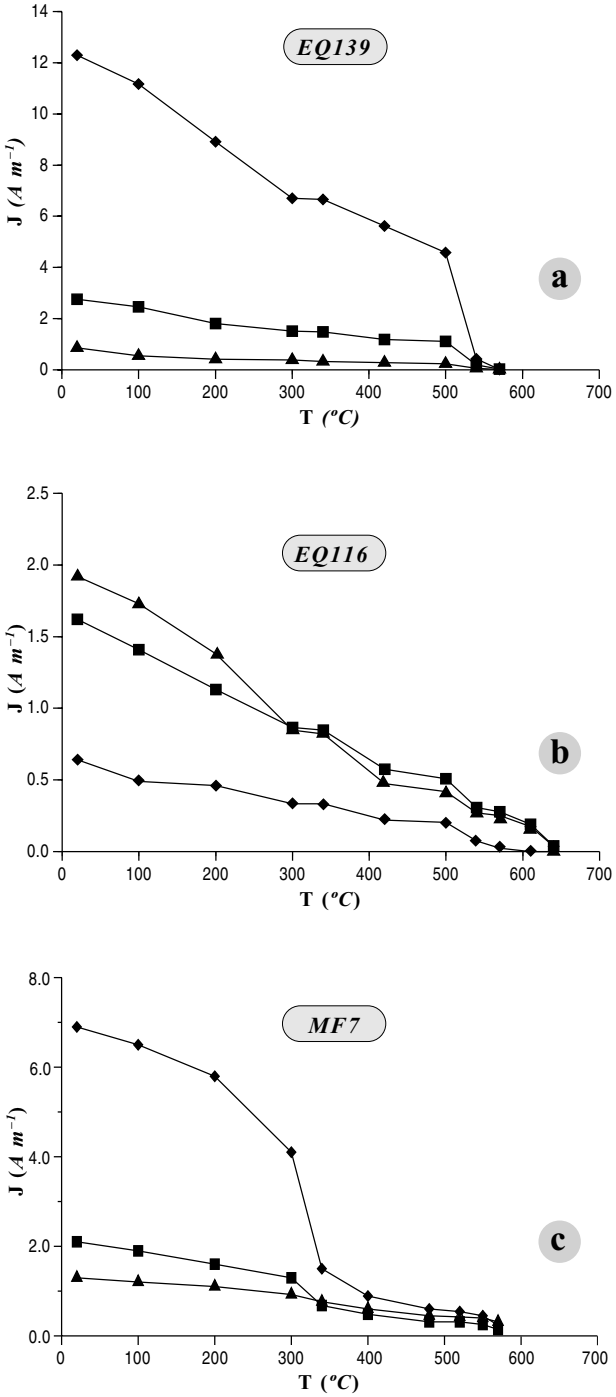


**Figure 6.** Thermal demagnetization of the IRM components acquired at 0.1, 0.5, 1.5 T (same specimens as in Fig. 5). Symbols: diamond: low-; square: intermediate-; triangle: high-coercivity component. In El Quemado, components are generally removed (a) below 600°C or secondly (b) at higher temperatures. In Marifil, (c) components are also removed at *c*. 580°C though a noticeable decrease of the low-coercivity component is observed between 300–400°C.

and shows no relation with the susceptibility which is usually low (66 to 2221 $\times$ $10^{-6}$ SI units). The NRM directions are mostly of reverse polarity and their dispersion is usually small. Two pilot specimens per site were stepwise demagnetized, one thermally and one in alternating field (AF). Magnetic susceptibility was measured after each heating step in order to detect possible mineralogical transformation. The median destructive field (MDF) is usually in the range 45 to 60 mT and the remanence intensity after heating up to 400–500°C is 90 to 100 per cent of the initial NRM value

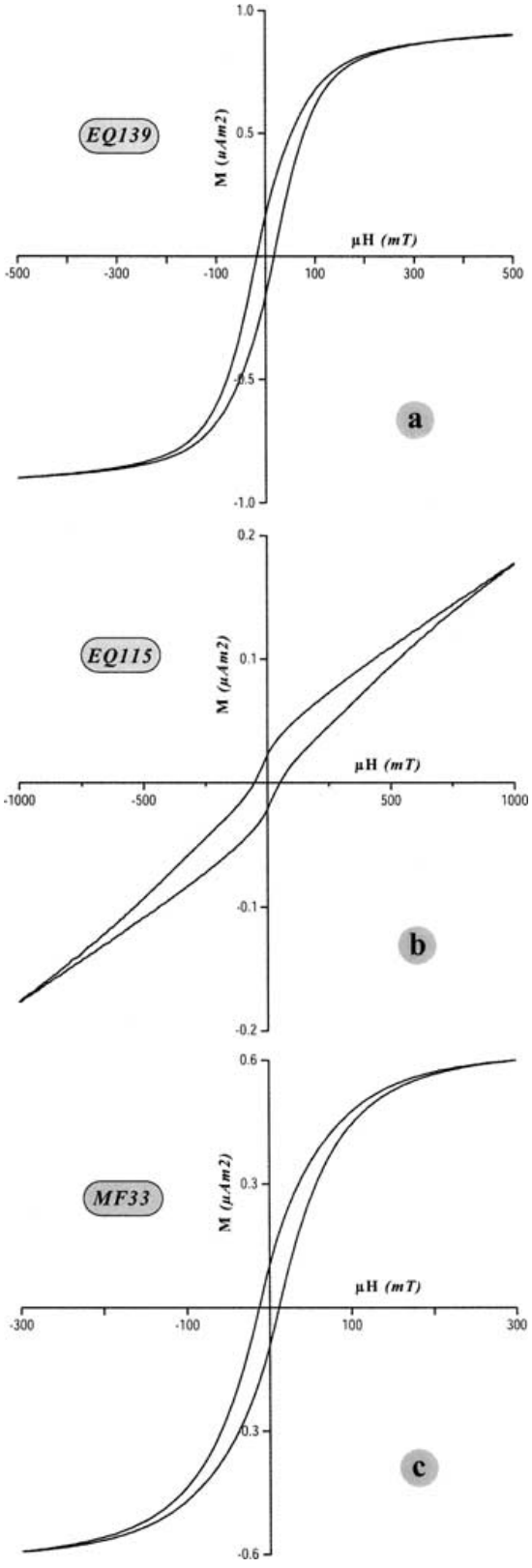


**Figure 7.** Representative hysteresis loops for El Quemado Complex (a: site F3b; b: site F1b) and Marifil Formation (c: site Cabo dos Bahías 1b). Geometries of El Quemado are (a) pot-belly indicative of Ti-magnetite and (b) wasp-waist indicative of Ti-magnetite plus haematite. In Marifil (c) the pot-belly geometry is widespread.

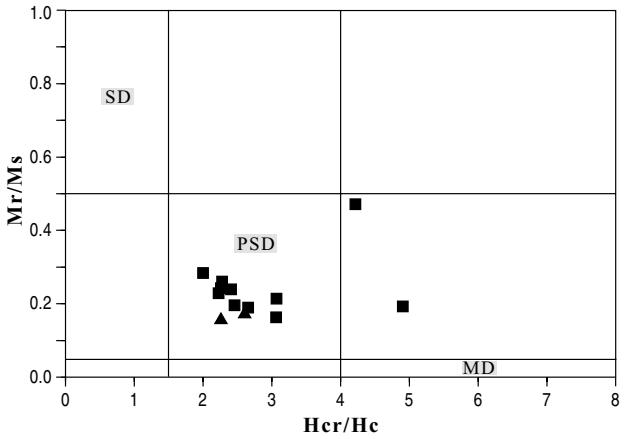


**Figure 8.** Day *et al.* (1977) plot of hysteresis parameters values for El Quemado Complex (squares) and Marifil Formation (triangles). Most of the samples fall in the pseudo-single domain field.

(Fig. 10). At most sites, secondary components are either absent or very weak and removed below 20–30 mT or 100–300°C. Thereafter, a characteristic component (ChRM) is isolated (Fig. 11) and completely erased at temperature higher than 550°C or peak-field usually of the order of 100 mT. Ignimbrites, lavas and tuffs show the same behaviour, apart a higher MDF for tuffs (70 to 170 mT). The thermal method was chosen at most sites for systematic demagnetization at 5 to 12 steps. The direction of the ChRM was calculated using the Kirschvink's (1980) principal component analysis at most sites and the great circle convergence method (McFadden & McElhinny 1988) at two sites characterized by susbstantial secondary components. At most sites the mean ChRM direction was calculated taking into account all the demagnetized specimens (Table 1) and its dispersion was usually very small ($\alpha_{95} < 5^\circ$ at 26 sites). At Lago Posadas both normal and reverse polarities occur and the reversal test (McFadden & McElhinny 1990) is positive, class 'C', critical angle $=11.4^\circ$ (Fig. 12a).

### *4.2.2 Marifil Formation*

The susceptibility (884 to 10855 $\times$ $10^{-6}$ SI) and NRM intensity ($10^{-2}$ to $10^{-1}$ A $m^{-1}$) values are usually higher than those of El Quemado (Table 1). The dispersion of the NRM directions is somewhat higher than for El Quemado, depicting both normal and reverse polarities. Stepwise demagnetization shows that the dispersion is due to strong secondary magnetization components at all sites but Cabo dos Bahías. They often account for more than 50 per cent of the initial NRM intensity and are completely removed at 400°C or 10–15 mT (Fig. 13). Systematic thermal or AF demagnetization was carried out with the same procedure as for El Quemado, resulting in site mean ChRM directions (Table 1) statistically well defined ($\alpha_{95} > 15^\circ$ at one site only). The reversal test (McFadden & McElhinny 1990) is positive, class 'C' critical angle=18.0° (Fig. 12b).

### *4.2.3 Virtual geomagnetic poles*

The southern VGP position was calculated from the ChRM direction of each site (Table 1, Fig. 14), leaving aside the 8 sites whose statistical parameters values were not satisfactory ($\alpha_{95} > 15^\circ$ or $k < 20$) and the site Ruta Cabo Raso 5a, which displays an anomalous

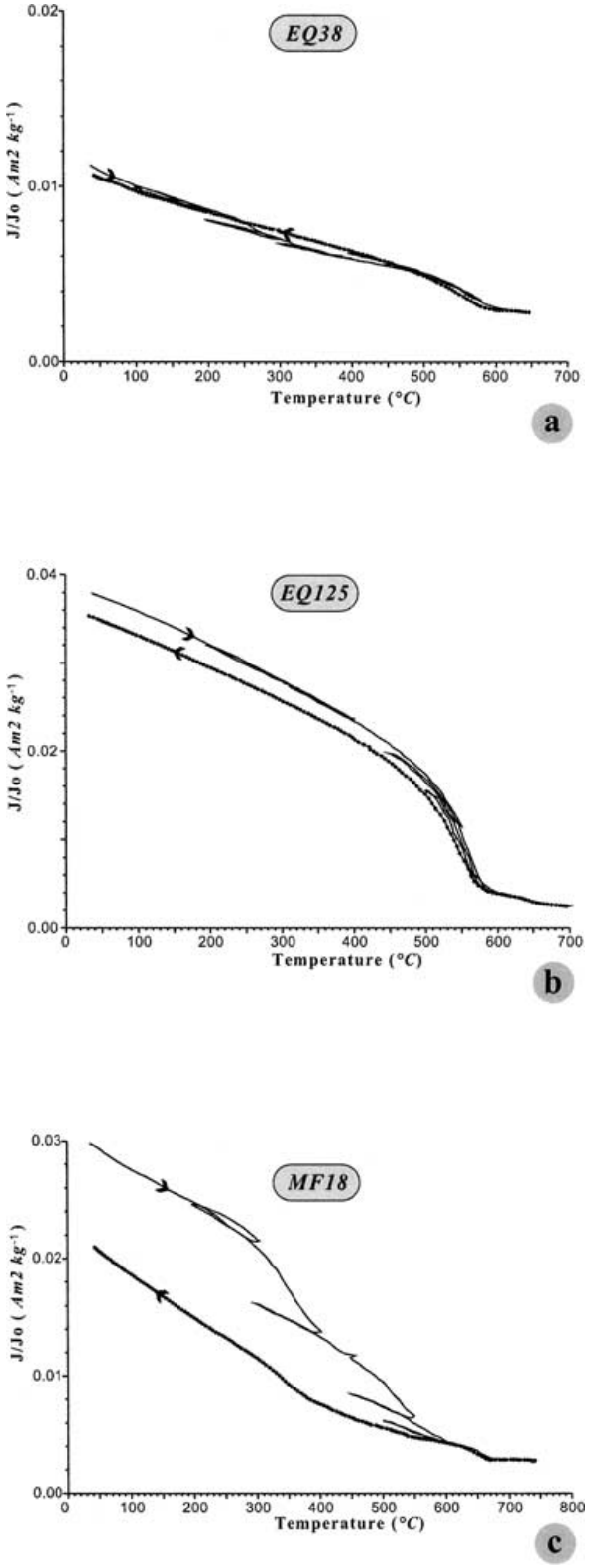


**Figure 9.** Thermomagnetic curves [J(T)] done in representative powders from El Quemado Complex (a: site M1a; b: F1a) and Marifil Formation (c: site Caleta Pedro 3b). In El Quemado, two sets of Curie temperatures are observed: (a) the widespread 550–580°C indicative of Ti-magnetite and less frequently (b) 620–670°C indicative of haematite/maghemite, example from F1a. In Marifil, a third Curie temperature at 350°C is indicative of Ti-rich magnetite.

inclination value (−88.6°). No structural correction was applied to the ChRM directions of the Marifil Formation, since in the Camarones region there is no field evidence for major structures within the volcanic rocks (Lema *et al.* 2001). Moreover, this formation belongs to the Somuncurá Massif, regarded as a structurally stable region. Therefore, it may be reasonably assumed that the effect of local tectonics, if any, is negligible. The mean VGP of the Marifil Formation is located at latitude 83°S, long. 138°E ($n = 10$, $A_{95} = 11.3°$) (Table 2). It improves the previous results by Creer *et al.* (1972) and is consistent with the palaeomagnetic pole Vizán (1998) has recalculated from the whole of the literature data of the Marifil Formation (Table 3).

The El Quemado Complex was sampled in the cordilleran foothills, where a complex compressional tectonics affected both the basement and the sedimentary cover since the Cretaceous. In order to derive the VGP position, ChRM direction must therefore be corrected according to the geological structure at the sampling site. This is not straightforward for volcanic rocks, which often lack primary depositional structures as bedding. The data used to calculate the tilt correction (Table 1) were derived taking into account both our field observations and the regional structural data (see chapter 2.3). At Lago Argentino, Lago San Martín South and Sierra Colorada, where the structural attitude varies from site to site, the correction strongly reduces the dispersion of the locality mean direction (Table 4) and the McFadden's (1990) fold test is positive at 95 per cent confidence level. ChRM was thus acquired prior to the Cretaceous tectonic deformation. The VGPs from the El Quemado fall in two groups, according to the latitude of the sampling localities (Fig. 14, Table 2). To the north of latitude 48°S (northern group = Sierra Colorada, Lago Posadas) they are similar to those from the Marifil Formation; to the south of 49°S (southern group = Lago San Martín North and South, Lago Argentino) they are displaced toward lower latitudes in the NE quadrant.

The remark by Roperch *et al.* (1997) that the ChRM inclinations in the Ibañez Formation (the equivalent of El Quemado in Chile) are lower than expected applies to the El Quemado Complex as well, in particular to the localities of the southern group. The possibility that the low inclinations are related to latitudinal displacement may be discarded on the grounds of regional geology (Roperch *et al.* 1997). The low inclination could be the result of either post-depositional processes which may occur in ignimbrites, as reomorphic flow and compaction, or incomplete averaging of paleosecular variation because of the small number of sites (4–5) at some locality. Lastly, accuracy of the tilt correction may be questioned if the rocks were emplaced upon an inclined palaeotopographical surface and the basic assumption of deposition onto a horizontal surface is not fulfilled. Even if the present data are not sufficient to give a definite explanation, the difference between the measured (Table 4) palaeomagnetic directions of the southern localities and that expected ($D = 192 \pm 11$, $I = 64 \pm 6$) based on the VGP location of the northern is too large to be caused solely by the possible, above mentioned sources of errors. Moreover, as discussed in the next section, the random nature of these errors is hardly compatible with the systematic pattern shown by the distribution of the El Quemado VGPs.

## 5 DISCUSSION

Statistically well defined ChRM directions of both normal and reverse polarity were found at most sites of the El Quemado Complex and Marifil Formation. They are mainly carried by PSD Ti-magnetite and stable up to temperatures close to the Curie point. The reversal and fold tests, where possible, are positive. The SEM and EDS

**Table 1.** Site mean palaeomagnetic data from El Quemado Complex and Marifil Formation. Symbols: n/N: total samples/selected samples; $k$: susceptibility; $Jr$: natural remanent magnetization intensity; ChRM: characteristic remanent magnetization; $D$, $I$: *in situ* declination, inclination; $D_t$, $I_t$: declination, inclination after tilt correction; $\alpha_{95}$: semi-angle of confidence; $k$: Fisher's precision parameter; VGP: southern virtual geomagnetic pole; Demagn.: demagnetization range in mT (AF) or °C (thermal); GC: great circles. Tilt correction: Strike follows the right-hand rule.

| Locality | Site | Lithology | n/N | $k$ | | ChRM | | | VGP | | Tilt cor. |
|---|---|---|---|---|---|---|---|---|---|---|---|
| Lat., Long. | | | | $10^{-6}$ SI | $J_r$ A m$^{-1}$ | $D$, $I$ | $D_t$, $I_t$ | $\alpha_{95}$ | $k$ | Lat S, Long E | Demagn. | Strike, dip |
| L. Argentino | Unión 1a | Tuff - D | 9/4 | 223 | $5.6\ 10^{-4}$ | 187.5, 53.7 | 136.0, 35.3 | 27.0° | 13 | – | AF 10–60 | 0, 50 |
| 50°11′S, 72°49′W | 1b | Tuff - D | 12/10 | 224 | $6.4\ 10^{-3}$ | 182.8, 63.7 | 123.3, 36.4 | 5.1° | 97 | 37°, 30° | Th 300–560 | " " |
| | Unión 2a | Tuff - D | 7/7 | 143 | $2.4\ 10^{-2}$ | 141.4, 52.8 | 127.0, 38.3 | 5.0° | 146 | 40°, 32° | Th 100–600 | 0, 20 |
| | 2b | Tuff | 12/12 | 238 | $3.0\ 10^{-2}$ | 149.0, 57.7 | 129.9, 44.4 | 3.0° | 204 | 45°, 30° | Th 300–545 | " " |
| | Unión 3a | Ignimbrite - R | 9/9 | 282 | $3.3\ 10^{-2}$ | 125.2, 44.0 | 151.6, 61.9 | 4.0° | 165 | 69°, 26° | Th 100–600 | 180, 26 |
| | 3b | Dacite | 12/11 | 243 | $2.1\ 10^{-3}$ | 111.0, 12.1 | 115.7, 36.1 | 6.4° | 59 | 32°, 24° | Th 400–555 | " " |
| L. San Martin, South | Maipu 1a | Dacite + Tuff | 23/23 | 124 | $3.7\ 10^{-2}$ | 188.1, 62.9 | 135.1, 56.1 | 3.5° | 77 | 55°, 21° | Th 200–650 | 353, 30 |
| 49°08′S, 72°30′W | 1b | Dacite | 8/8 | 189 | $5.4\ 10^{-2}$ | 7.5, −63.4 | 314.1, −56.1 | 3.2° | 301 | 55°, 21° | AF 20–60 | " " |
| | Maipu 2a | Ignimbrite - RD | 10/10 | 2221 | $2.9\ 10^{-1}$ | 145.5, 65.5 | 139.8, 56.0 | 2.2° | 400 | 58°, 26° | Th 300–650 | 34, 10 |
| | 2b | Ignimbrite - RD | 8/8 | 1914 | $6.7\ 10^{-2}$ | 130.5, 64.3 | 128.8, 54.3 | 2.5° | 511 | 50°, 19° | Th 530–585 | " " |
| | Maipu 3a | Rhyodacite | 11/11 | 264 | $1.7\ 10^{-2}$ | 127.1, 24.6 | 126.7, −15.1 | 18.4° | 7 | – | Th 200–580 | 30, 40 |
| | 3b | Granodiorite | 10/10 | 288 | $2.5\ 10^{-3}$ | 119.8, 82.8 | 120.0, 42.8 | 12.9° | 15 | – | Th 380–560 | " " |
| L. San Martin, North | Chacabuco 1a | Arkose | 6/4 | 75 | $2.4\ 10^{-4}$ | 356.9, −66.7 | 341.7, −60.1 | 17.4° | 29 | – | AF 10–50 | 30, 10 |
| 49°02′S, 72°14′W | 1b | Arkose | 5/3 | 114 | $7.8\ 10^{-4}$ | 349.0, −69.5 | 334.2, −62.0 | 18.4° | 46 | – | Th 200–560 | " " |
| | Chacabuco 2a | Ignimbrite - R | 6/6 | 291 | $5.1\ 10^{-3}$ | 166.2, 57.5 | 157.1, 50.0 | 4.2° | 256 | 65°, 56° | Th 500–600 | " " |
| | 2b | Ignimbrite - R | 7/7 | 223 | $2.2\ 10^{-2}$ | 175.8, 54.5 | 166.1, 48.2 | 4.6° | 176 | 68°, 75° | AF 30–80 | " " |
| | Chacabuco 3a | Rhyolite | 8/8 | 66 | $4.7\ 10^{-3}$ | 156.7, 58.6 | 149.1, 50.2 | 2.5° | 475 | 61°, 44° | Th 500–600 | " " |
| | 3b | Rhyolite | 9/9 | 156 | $6.4\ 10^{-3}$ | 143.3, 56.0 | 138.8, 46.7 | 2.3° | 510 | 52°, 36° | AF 30–70 | " " |
| L. Posadas | Furioso 1a | Ignimbrite - R | 8/8 | 117 | $1.8\ 10^{-3}$ | 7.1, −55.6 | 28.9, −54.8 | 2.6° | 450 | 65°, 179° | Th 500–600 | 195, 15 |
| 47°27′S, 71°48′W | 1b | Ignimbrite - R | 12/12 | 102 | $1.4\ 10^{-2}$ | 179.8, 65.8 | 213.5, 65.3 | 2.9° | 232 | 68°, 211° | Th 450–565 | " " |
| | Furioso 2a | Ignimbrite - R | 6/6 | 681 | $9.4\ 10^{-2}$ | 148.7, 54.4 | 169.0, 63.4 | 8.2° | 68.2 | 82°, 32° | AF 20–200 | " " |
| | 2b | Ignimbrite - R | 11/11 | 1088 | $1.5\ 10^{-1}$ | 139.4, 56.1 | 158.9, 67.0 | 1.9° | 573 | 76°, 1° | AF 30–80 | " " |
| | Furioso 3a | Ignimbrite - R | 8/8 | 485 | $5.9\ 10^{-2}$ | 156.2, 46.6 | 172.0, 54.4 | 2.6° | 438 | 76°, 80° | Th 350–580 | " " |
| | 3b | Ignimbrite - R | 10/10 | 705 | $8.1\ 10^{-2}$ | 161.1, 46.2 | 177.3, 53.2 | 2.2° | 484 | 76°, 99° | AF 20–80 | " " |
| | Furioso 4a | Ignimbrite - D | 10/3 | 141 | $1.7\ 10^{-2}$ | 355.6, −59.2 | 21.9, −60.9 | 23.7° | 28 | – | Th 450–580 | " " |
| | 4b | Ignimbrite - D | 10/10 | 99 | $9.7\ 10^{-4}$ | 347.0, −58.4 | 12.9, −62.4 | 5.1° | 91 | 80°, 180° | Th 350–530 | " " |
| | Furioso 5a | Tuff, reworked | 6/0 | 167 | $1.3\ 10^{-3}$ | dispersed | – | – | – | – | – | – |
| | 5b | Tuff, reworked | 12/11 | 104 | $1.5\ 10^{-3}$ | 189.8, 62.1 | 216.9, 59.8 | 9.7° | – | 63°, 197° | Th 100–550 (GC) | " " |
| | Furioso 6a | Tuff, reworked | 11/9 | 38 | $1.0\ 10^{-4}$ | 351.4, −60.8 | 19.8, −63.3 | 11.7° | 20 | 76°, 195° | Th 300–580 | " " |
| | 6b | Ignimbrite - RD | 11/10 | 84 | $2.3\ 10^{-3}$ | 184.7, 61.5 | 212.2, 60.6 | 5.9° | – | 66°, 196° | Th 20–520 (GC) | " " |
| Sierra Colorada | Roballos 1a | Ignimbrite - RD | 5/5 | 223 | $6.5\ 10^{-2}$ | 153.3, 62.4 | 172.7, 66.2 | 3.0° | 644 | 85°, 2° | Th 100–580 | 185, 10 |
| 47°23′S, 71°44′W | 1b | Rhyolite | 5/5 | 279 | $8.1\ 10^{-2}$ | 148.3, 57.6 | 163.6, 62.5 | 3.3° | 549 | 78°, 29° | AF 30–100 | " " |
| | Roballos 2a | Ignimbrite - D | 11/11 | 513 | $9.5\ 10^{-2}$ | 230.8, 37.7 | 203.4, 49.6 | 2.1° | 456 | 65°, 163° | Th 100–600 | 15, 30 |
| | 2b | Ignimbrite - D | 9/9 | 1218 | $1.5\ 10^{-1}$ | 208.8, 43.4 | 179.7, 43.0 | 2.0° | 675 | 68°, 108° | AF 40–80 | " " |
| | Roballos 3a | Ignimbrite - R | 22/22 | 1017 | $3.9\ 10^{-1}$ | 129.1, 30.1 | 207.8, 63.8 | 4.6° | 47 | 71°, 203° | Th 200–580 | 190, 65 |
| | 3b | Ignimbrite - R | 7/7 | 1225 | $4.6\ 10^{-1}$ | 128.6, 31.4 | 210.8, 64.1 | 4.0° | 232 | 69°, 206° | AF 40–100 | " " |
| Bahia Camarones | Cabo Dos Bahías 1a | Trachi-rhyolite | 6/6 | 7681 | $5.0\ 10^{-2}$ | 357.3, −54.6 | – | 6.0° | 126 | 80°, 102° | AF 10–100 | – |
| 44°45′S, 65°35′W | 1b | Trachi-rhyolite | 10/10 | 884 | $5.3\ 10^{-2}$ | 200.2, 68.2 | – | 3.5° | 190 | 75°, 238° | AF 60–100 | – |
| | Belvedere 2a | Trachi-rhyolite | 4/4 | 5752 | 15.5 | 18.5, −45.6 | – | 6.4° | 205 | 67°, 161° | AF 40–100 | – |
| | 2b | Trachi-rhyolite | 12/10 | 2069 | $9.8\ 10^{-2}$ | 33.3, −62.4 | – | 2.5° | 366 | 66°, 214° | Th 400–620 | – |
| | Caleta Pedro 3a | Ignimbrite - T | 5/5 | 1857 | $3.7\ 10^{-2}$ | 8.9, −58.2 | – | 2.9° | 703 | 81°, 166° | AF 10–70 | – |
| | 3b | Ignimbrite - T | 9/9 | 1535 | $2.8\ 10^{-2}$ | 24.9, −54.5 | – | 8.5° | 37 | 69°, 186° | Th 350–550 | – |
| | Caleta Sara 4a | Ignimbrite - T | 5/4 | 5085 | $5.8\ 10^{-1}$ | 158.8, 38.2 | – | 14.5° | 41 | 61°, 71° | AF 10–30 | – |
| | 4b | Ignimbrite - T | 10/10 | 1024 | $1.0\ 10^{-2}$ | 339.3, −58.0 | – | 3.7° | 169 | 73°, 39° | Th 450–550 | – |
| | Ruta Cabo Raso 5a | Rhyolite | 5/5 | 9701 | $8.3\ 10^{-2}$ | 345.5, −88.6 | – | 3.0° | 649 | – | AF 10–50 | – |
| | 5b | Rhyolite | 9/7 | 8018 | $6.1\ 10^{-2}$ | 335.0, −55.7 | – | 11.5° | 28 | 69°, 40° | Th 320–480 | – |
| | Las Lajas 6a | Rhyolite | 6/6 | 10855 | $1.7\ 10^{-1}$ | 187.7, 58.1 | – | 4.3° | 248 | 82°, 161° | AF 20–100 | – |
| | 6b | Rhyolite | 11/11 | 3968 | $1.3\ 10^{-1}$ | 196.5, 70.8 | – | 21.5° | 6 | – | Th 440–550 | – |

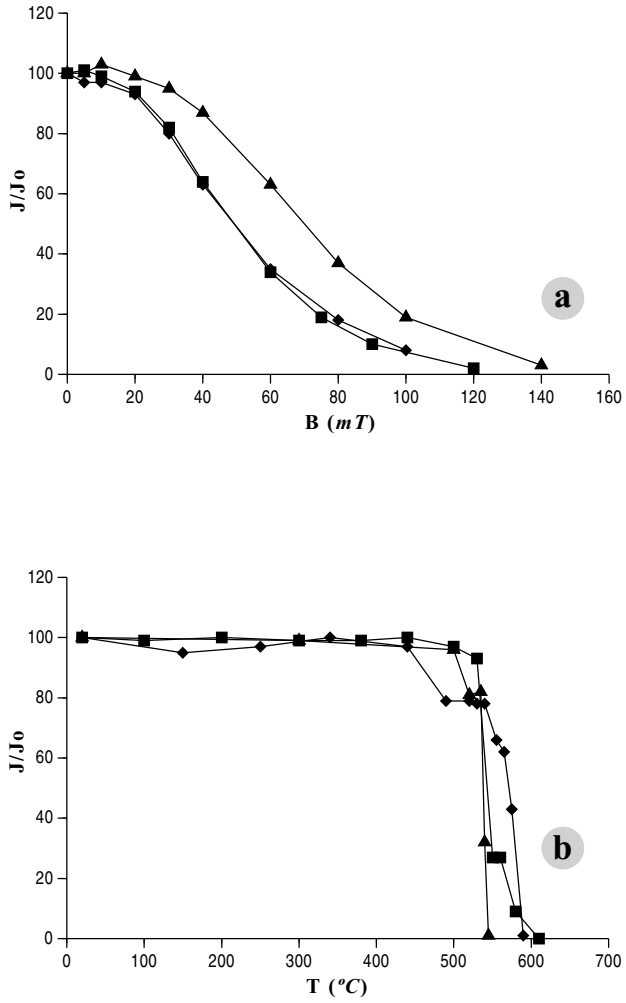


**Figure 10.** Normalized intensity decay curves for AF (a) and thermal (b) demagnetization, El Quemado Complex. Symbols: triangle = tuff, site U2b; square = lava, site M1b; diamond = ignimbrite, site R2b.

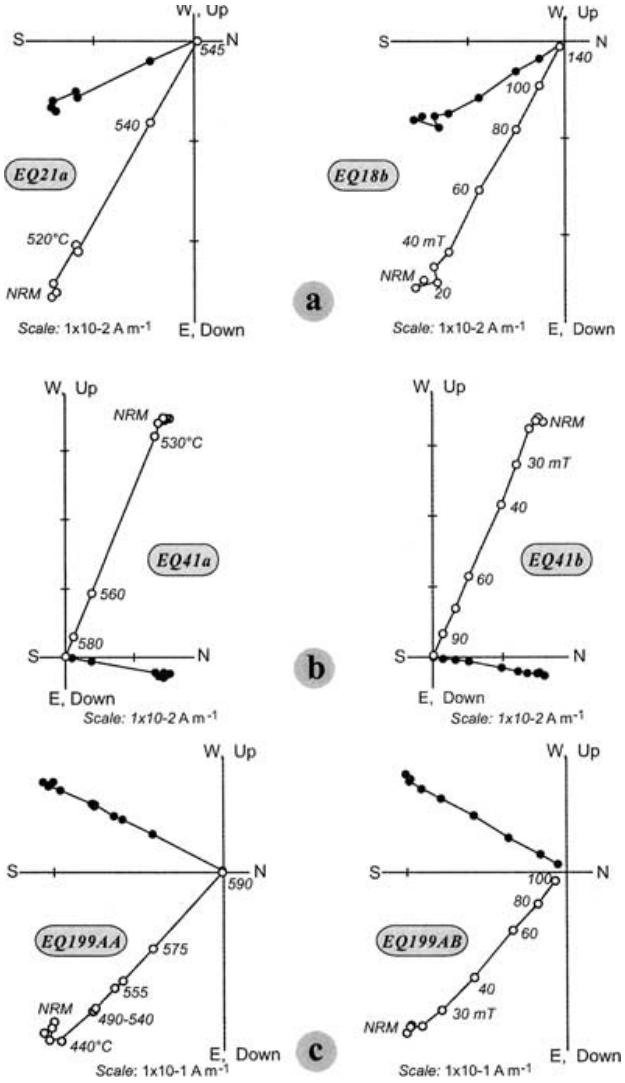


**Figure 11.** Zijderveld (1967) diagrams (geographic reference system) for thermal and AF demagnetization in sister specimens (same as in Fig. 10). Top = tuff; middle = lava; bottom = ignimbrite. Symbols: full dot = declination; open dot = apparent inclination; figures = temperature (°C) or peak-field (mT) value.

analyses show that most of the alteration of the Fe–Ti oxides occurred above 600°C, i.e. at the same time as the rocks emplacement. These results point to a primary origin of the ChRM, whose direction can be reasonably assumed to parallel the direction of the Earth's magnetic field during cooling of the rocks. The VGPs of the Marifil Formation are consistent with the others middle Jurassic VGPs from Patagonia, whereas those of El Quemado show an elongated distribution (Fig. 14). Following a suggestion by M. Beck, we analyse it using the shape analysis technique (Beck 1999; Beck *et al.* 2000). The first step consists in calculating the elongation of the VGP set, defined as $E = k_2/k_3$, where $k_2$ and $k_3$ are the eingenvectors of the Bingham statistics (Schmidt 1990; Beck 1999). A small elongation value may depend on the direction-to-pole mapping relationship (Butler 1992) and the various errors which may affect the data at each site (not fully accurate tilt correction, incomplete averaging of palaeosecular variation, ....). A high value shows that some geological process biased the VGPs distribution, whose shape is a clue to trace back the process.

The elongation of the El Quemado data set is very high, $E = 13.4$ and is mainly due to the shifting of the southern group VGPs relative to those of the northern group (Fig. 14). This systematic difference suggests to analyse separately the two sub-sets. The 16 VGPs of the El Quemado northern group are not far from each other, their elongation ($E = 3.6$) is moderate and that of the corresponding ChRM directions ($E = 2.0$) is close to circularity. The VGPs distribution is thus hardly related to a definite geological cause and this conclusion is substantiated by the fact that their mean pole (81°S, 172°E; $A_{95} = 7.6°$) is indistinguishable from those of the Marifil and Chon Aike formations (Table 3, Fig. 15). These results show that the APW path of South America was very limited during the emplacement of the three main units of the Patagonian volcanic province approximately from 185 to 155 Ma, and that no major intracontinental movements occurred since between extra-Andean Patagonia and the Andean Cordillera foothills region to the north of 48°S. No evidence for such movements also results from the Ibañez Formation (the Chilean equivalent of El Quemado) in the vicinity of Lago Carrera, some 100 km to the NW of our localities (Roperch *et al.* 1997). The northern region of Lago Posadas–Sierra Colorada may thus be regarded as stable and its mean pole used as a reference for

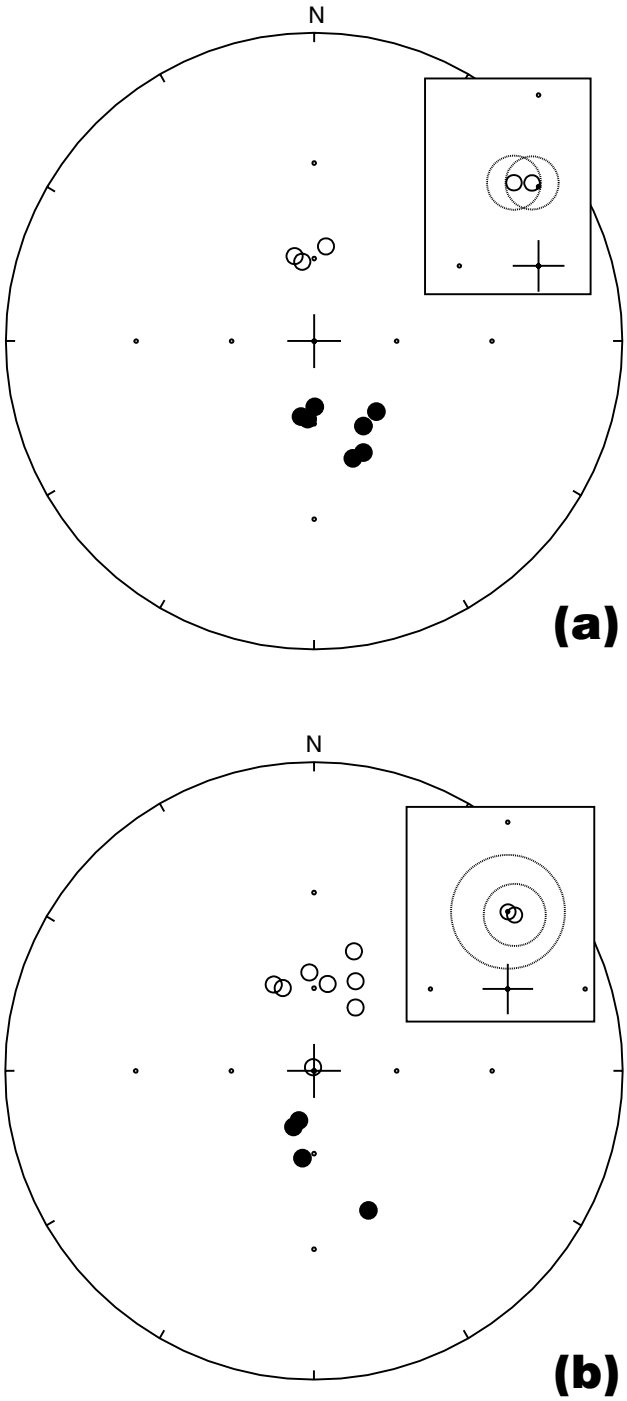


**Figure 12.** Positive Reversal tests in (a) El Quemado Complex at Lago Argentino and (b) Marifil Formation at Camarones (see also text).

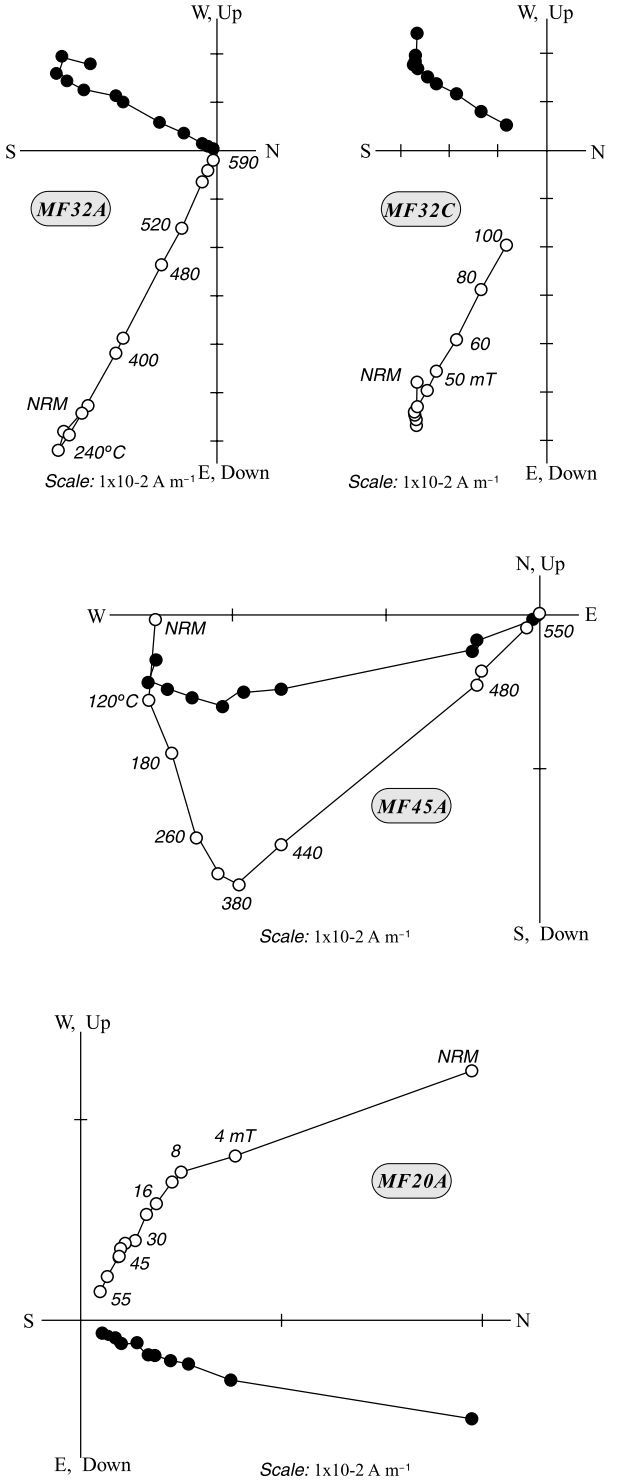


**Figure 13.** Zijderveld (1967) diagrams (geographic reference system) for thermal and AF demagnetization, Marifil Formation (symbols as in Fig. 11). Top = site Cabo dos Bahias 1b; middle = Las Lajas 6b; bottom = Caleta Pedro 3b.

the southern group of VGPs. The elongation of this group is high, $E = 6.0$, and approximately perpendicular to the palaeomeridian through the sampling region and the reference pole (Fig. 16). Beck *et al.* (2000) have remarked that in-situ rotation about a vertical axis changes only the ChRM declination and causes the corresponding VGP to move perpendicular to the palaeomeridian along a small circle centred close to the sampling site. The small circle that best fits the VGPs of the El Quemado (Fig. 16) is centred at 19.2°S, 296.3°E, radius =77.3°, not far from our sampling area. The shape of the VGPs distribution favours therefore the hypothesis that counterclockwise differential block rotations around a vertical axis occurred in the region between Lago Argentino and Lago San Martín relative

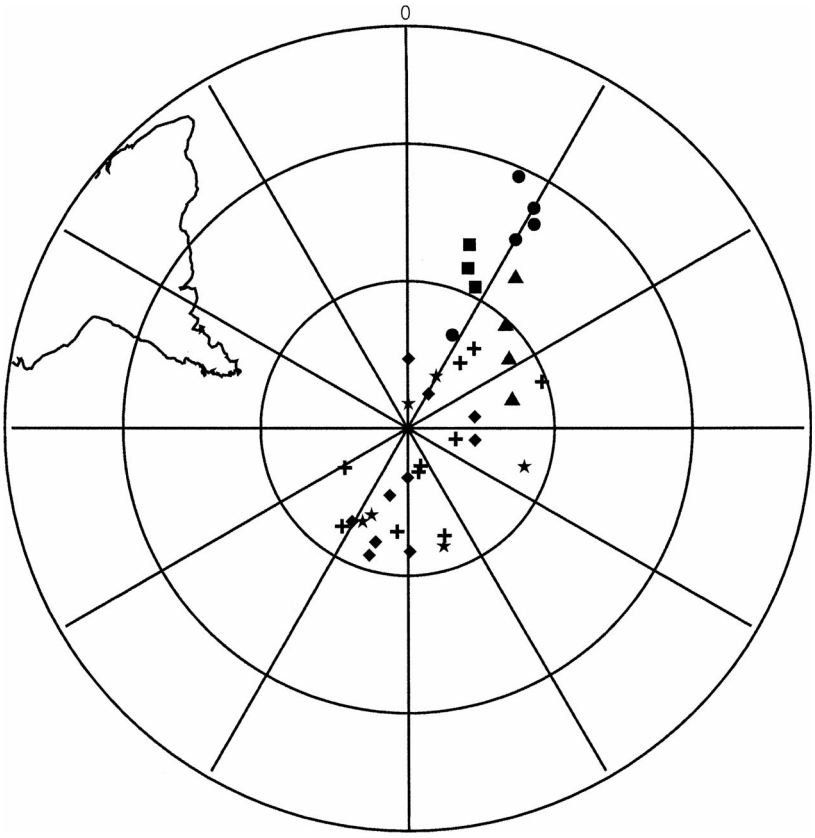


**Figure 14.** Site virtual geomagnetic poles (VGPs) for El Quemado Complex and Marifil Formation (see also text). Symbols: circle = Lago Argentino; square = Lago San Martín South; triangle = Lago San Martín North; diamond = Lago Posadas; star = Sierra Colorada; cross = Bahía Camarones.

to Lago Posadas–Sierra Colorada. The amount of rotation increases (Table 5) from *c*.40° at lago San Martín North to *c*.65° at Lago Argentino.

The literature palaeomagnetic data for the region of the present study consist of only two sites close to the locality Lago San Martín North (Burns *et al.* 1980). The results of one site are fully consistent with ours, whereas the other yielded a ChRM direction strongly deviated eastwards. More to the south, counter-clockwise rotations up to 90° have been found in Mesozoic rocks of the Patagonian Cordillera (Dalziel *et al.* 1973; Burns *et al.* 1980; Cunnigham *et al.* 1991). These rotations qualitatively support the concept of oroclinal bending of the Southernmost Andes, but data are too scanty to test a relationship between the rotation amount, the age of rocks and the sampling sites location.

**Table 2.** Locality VGPs from the El Quemado Complex and Marifil Formation. Symbols: *n*: number of sites; $A_{95}$: semi-angle of confidence.

| Locality | *n* | VGP Lat., Long. | $A_{95}$ |
|---|---|---|---|
| **El Quemado Complex** | | | |
| *South of 49 °S* | | | |
| Lago Argentino | 5 | 45°S, 29°E | 14° |
| Lago San Martin South | 4 | 55°S, 22°E | 4° |
| Lago San Martin North | 4 | 62°S, 50°E | 12° |
| *North of 49 °S* | | | |
| Lago Posadas | 10 | 80°S, 178°E | 10° |
| Sierra Colorada | 6 | 81°S, 161°E | 15° |
| All | 16 | 81°S, 172°E | 8° |
| **Marifil Formation** | | | |
| Bahía Camarones | 10 | 83°S, 138°E | 11° |

In addition, many studies carried out in fold and thrust belts from Europe (e.g. McClelland & McCaig 1989; Oldow *et al.* 1990; Allerton 1998) and North America (Schwartz & Van der Voo 1984), demonstrated that thrusts are likely to produce rotations in the directions of the remanent magnetization around vertical axes. Rotations around vertical axes commonly occur (see Boyer & Elliot 1982; Allerton 1998) by differential shortening along strike and/or when a new thrust sheet climbs onto another using lateral ramps. This will cause the new thrust sheet to translate at the same time it rotates. These processes affect more intensely the internal (older) part of the orogenic wedge, whereas rotations hardly develop at the advancing front (McClelland & McCaig 1989; Allerton 1998).

Our sampling localities are located from south to north, at progressively greater distance from the inner (western) part of the orogenic wedge (*cf.* Ramos 1989, Fig. 4; Kraemer *et al*. 2002, Fig. 6). This can explain why we find progressively decreasing amounts of rotations in the south between Lago Argentino and Lago San Martín North and finally hardly any rotation in northern Lago Posadas–Sierra Colorada, located almost at the front of the thrust and fold belt.

## 6 CONCLUSIONS

The Jurassic rocks of the Patagonian volcanic province were sampled at five localities in the cordilleran foothills of southern Patagonia (El Quemado Complex) and one in the Somuncurá Massif of extra-Andean Patagonia (Marifil Formation). The mean VGP (83°S,

**Table 3.** Jurassic palaeomagnetic poles (PPs) for Patagonia (Fig. 14). $A_{95}$ ($dp/dm$): confidence limits of the pole; (∗) age from Pankhurst *et al.* (2000).

| Rock unit | Lithology | Age (Ma)/Stage | Lat. S | Long. E | $A_{95}$ $dp/dm$ | Reference |
|---|---|---|---|---|---|---|
| 1-Cañadón Asfalto Basin | Sediments | Late Jurassic Neocomian | 68.5° | 201° | 5.7°/7.8° | Guena *et al.* (2000) |
| 2-El Quemado Complex (N of 48°S) | Volcanics | 153–157 (∗) | 81° | 172° | 7.6° | This study |
| 3-Chon Aike Fm. | Volcanics | 162–172 (∗) | 81° | 207° | 13.5° | Recalculated in Vizán (1998) |
| 4-Mamil Choique | Dykes | 170 | 70° | 190° | 9.7° | Rapalini & López de Luchi (2000) |
| 5-Marifil Fm. | Volcanics | 178–188 (∗) | 80.5° | 203.5° | 8.7° | Recalculated in Vizán (1998) |
| 6-Marifil Fm. | Volcanics | 178–188 (∗) | 83° | 138° | 11.3° | This study |
| 7-Lepá–Osta Arena Fm. | Volcanics-Sediments | Pliensbachian-Toarcian | 75.5° | 129° | 6.8° | Vizán (1998) |
| 8-Neuquén Basin | Sediments/Volcanics | Pliensbachian-Toarcian | 81° | 92° | 2.7° | Iglesia Llanos (1997) |
| 9-Neuquén Basin | Sediments | Hettangian-Sinemurian | 56° | 235° | 4.0° | Iglesia Llanos (1997) |

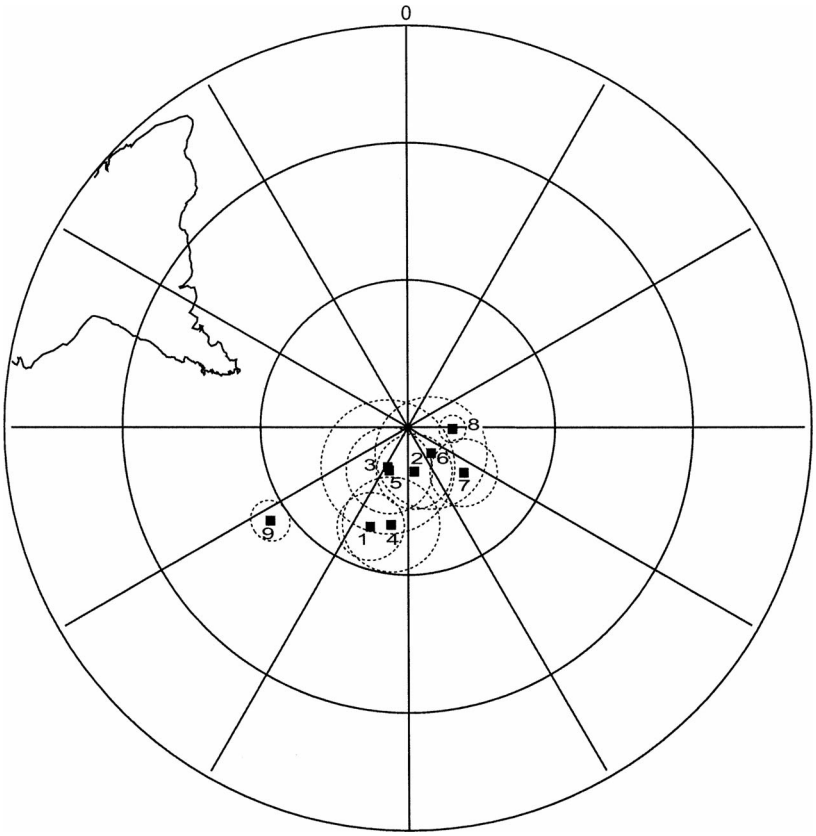


**Figure 15.** Jurassic palaeomagnetic poles for Patagonia (numbers refer to Table 3).

138°E; $n = 10$, $A_{95} = 11°$) of the middle Jurassic Marifil Formation agrees well with the literature data from Patagonia and stable South America. The VGPs of the upper Jurassic El Quemado Complex fall in two groups. The localities to the north of latitude 48°S yield a mean VGP (81°S, 172°E; $n = 16$, $A_{95} = 8°$) indistinguishable from that of the Marifil Formation. Those south of 49°S yield a highly elongated VGP distribution, whose shape may be the result of counter-clockwise rotation about vertical axes. Three main conclusions can be drawn from these results.

**Table 4.** Statistical parameters for the fold test. Symbols: n: number of sites; D, I: locality mean declination, inclination; $\alpha_{95}$: semi-angle of confidence; $\xi$, $\xi_{95\,\text{per cent}}$ : test statistic, critical value at 95 per cent (McFadden 1990).

| Locality | | $n$ | $D$, $I$ | $\alpha_{95}$ | $\xi$ | $\xi_{95\,\text{per cent}}$ |
|---|---|---|---|---|---|---|
| Lago Argentino | *in situ* | 5 | 135.1, 48.8 | 26.2° | 4.9 | 2.6 |
| | unfolded | ” | 127.4, 43.8 | 13.2° | 1.2 | ” |
| Lago San Martín South | *in situ* | 4 | 163.8, 66.3 | 14.4° | 0.8 | 2.3 |
| | unfolded | ” | 134.4, 55.7 | 3.1° | 1.1 | ” |
| Sierra Colorada | *in situ* | 6 | 164.3, 51.7 | 29.8° | 4.1 | 2.9 |
| | unfolded | ” | 189.7, 59.4 | 11.5° | 0.1 | ” |

(1) the regions of the Marifil Formation and the northernmost El Quemado Complex can be regarded as part of stable South America, whose APW path was limited during the emplacement of the volcanic rocks of Patagonia (185 to 155 Ma).

(2) the palaeomagnetic data from the El Quemado Complex evidence large N–S changes along the Patagonian Cordillera, with stable areas in the north (Lago Posadas, Sierra Colorada) and considerable amounts of counter-clockwise rotation in the south (Lago San Martín, Lago Argentino).

(3) the amount of rotation seems to be related to the position of the sampling areas in the thrust and fold belt. Thus, when the locality is close to the inner part of the orogenic wedge where

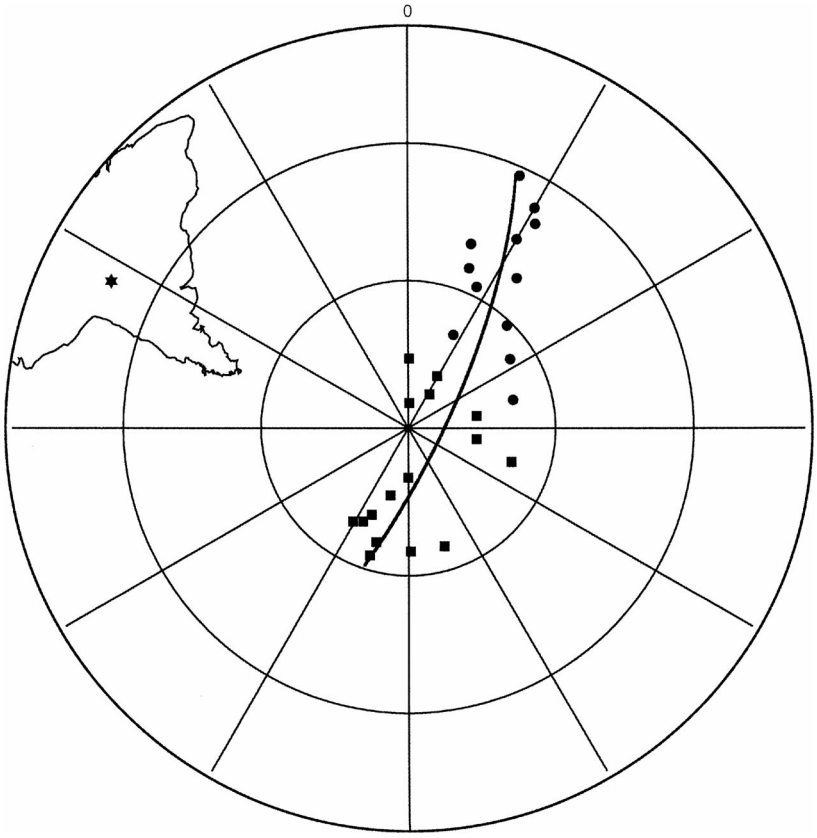


**Figure 16.** Distribution of the northern 'stable' (squares) and southern 'rotated' (circles) VGPs from El Quemado. We used the shape analysis method (Beck 1999; Beck *et al.* 2000), to determine if the elongation of the VGPs population is caused by the direction-to-pole mapping relationship or else, by tectonic rotations around vertical axis. The centre of the best-fitting small circle is (star) at 19.2°S, 296.3°E.

**Table 5.** Rotations calculated in the studied localities, following Beck *et al.* (1986). Lat. RP: latitude of the Reference Pole (last column); Lon. RP: longitude of the Reference Pole; Lat. CP: latitude of the locality calculated Pole; Lon. CP: longitude of the locality calculated Pole; $A_{95}$-RP: confidence angle of Reference Pole; $A_{95}$: confidence angle of the locality calculated Pole; Rot.: counter clockwise rotation around a vertical axis; ΔR: Rotation Error; Ref. Pole: Reference Poles in Table 3; CP: calculated locality pole in Table 2.

| Locality | Lat. RP (°S) | Lon. RP (°E) | Lat. CP (°S) | Lon. CP (°E) | $A_{95}$-RP | $A_{95}$ | Rot. | ΔR | Ref. Pole |
|---|---|---|---|---|---|---|---|---|---|
| *Lago Argentino* | 81 | 172 | 45 | 29 | 7.6° | 14° | 61.6° | 15.2° | *2* |
| *San Martín South* | 81 | 172 | 55 | 22 | 7.6° | 4° | 56.6° | 9.5° | *2* |
| *San Martín North* | 81 | 172 | 62 | 50 | 7.6° | 12° | 38.7° | 14.0° | *2* |
| *Camarones* | 81 | 204 | 83 | 138 | 8.7° | 11° | 8.0° | 14.8° | *5* |

compression was more intense (i.e. Lago Argentino), rotation is greatest. Conversely, when the locality is close to the front of the thrust and fold belt (i.e. Lago Posadas–Sierra Colorada) rotations, if any, are imperceptible.

## ACKNOWLEDGMENTS

This paper is dedicated to Raffaella Ruffini in memory of her merits as a skillful scientist and a wonderful person. The work was financed through the Italian Antarctic National Research Programme (R. Lanza, M.A. Laurenzi) and the National Research Council of Argentina (CONICET-PIP 4735/96, A.C. Riccardi). M.P. Iglesia Llanos acknowledges receipt of a CONICET post-doctoral fellowship while at Utrecht laboratory. Special thanks are given to F. Da Roit and T. Mullender for their skilfull laboratory assistance, and P.E. Kraemer for his comments and suggestions. The manuscript greatly benefited from the reviews of an anonymous referee and M. Beck, who introduced us to the VGP shape analysis and helped with calculations.

## REFERENCES

Allerton, S., 1998. Geometry and kinematics of vertical-axis rotations in fold and thrust belts, *Tectonophysics,* **299,** 15–30.

Alric, V.I., Haller, M.J., Féraud, G., Bertrand, H. & Zubia, M., 1996. Cronología $^{40}Ar/^{39}Ar$ del volcanismo jurásico de la Patagonia extrandina, *XIII Cong. Geol. Argent.,* Actas **5,** 243–250.

Arbe, H.A., 1988. El Cretácico de la Cuenca Austral: sus ciclos de sedimentación, Universidad de Buenos Aires, Buenos Aires, p. 334.

Beck, M.E., Jr, 1999. On the shape of paleomagnetic data sets, *J. geophys. Res.,* **104,** 25 427–25 441.

Beck, M.E., Jr, Drake, R. & Butler, R.E., 1986. Paleomagnetism of Cretaceous volcanic rocks from central Chile and implications for the tectonics of the Andes, *Geology,* **14,** 132–136.

Beck, M., Jr, Burmester, R., Cembrano, J., Drake, R., García, A., Hervé, F. & Munizaga, F., 2000. Paleomagnetism of the North Patagonian batholith, southern Chile. An exercise in shape analysis, *Tectonophysics,* **326,** 185–202.

Bertrand, H., Féraud, G., Haller, M., Luais, B., Martinez, M., Alric, V. & Fornari, M., 1999. The Mesozoic silicic large igneous province of Patagonia: chronology and origin evidenced by $^{40}$Ar-$^{39}$Ar dating and Sr-Nd isotopes, *2nd South Am. Symp. Am. Isotopic Geology,* Actas, 167–169.

Bonarelli, G. & Nágera, J.J., 1921. Observaciones geológicas en las inmediaciones del lago San Martín (Territorio de Santa Cruz), *Bol. Dir. Gen. Minas,* Buenos Aires, **27B,** 1–39.

Boyer, S. & Elliot, D., 1982. Thrust Systems, *Am. Assoc. Petr. Geol. Bull.,* **66,** 1196–1230.

Burns, K.L., Rickard, M.J., Belbin, L. & Chamalaun, F., 1980. Further palaeomagnetic confirmation of the Magellanes orocline, *Tectonophysics,* **63,** 75–90.

Butler, R.F., 1992. Paleomagnetism, Blackwell Scientific Publications, Oxford, p. 319.

Camacho, H.H., 1979. Descripción geológica de la Hoja 47h–47g, Bahía Camarones, *Serv. Geol. Nac.,* Buenos Aires, Bol. **153,** 1–29.

Carmichael, C.M., 1967. The iron-titanium oxides of salic volcanic rocks and their associated ferromagnesian silicates, *Contr. Min. Petrol.,* **14,** 36–64.

Cas, R.A.F. & Wright, J.V., 1987. *Volcanic Successions: Modern and Ancient*. Allen & Unwin, London,

Creer, K.M., Mitchell, J.G. & Abou Deeb, J., 1972. Palaeomagnetism and radiometric age of the Jurassic Chon Aike Formation from Santa Cruz province, Argentina: implications for the opening of the South Atlantic, *Earth planet. Sci. Lett.,* **14,** 131–138.

Cunnigham, D.W., Klepeis, K.A., Gose, W.A. & Dalziel, I.W.D., 1991. The patagonian orocline: new paleomagnetic data from the Andean magmatic arc in Tierra del Fuego, Chile, *J. geophys. Res.,* **96,** 16 061–16 067.

Dalziel, I.W.D., Kligfield, R., Lowrie, W. & Opdyke, N.D., 1973. Palaeomagnetic data from the southernmost Andes and the Atarctandes, in *Implications of Continental Drift to The Earth Sciences,* pp. 37–101, eds Tarling, D.H. & Runcorn, S.K., Academic Press, London.

Day, R., Fuller, M. & Schmidt, V.A., 1977. Hysteresis properties of titanomagnetites: grain size and compositional dependance, *Phys. Earth planet. Inter.,* **13,** 260–267.

Delvigne, J.E., 1998. Atlas of micromorphology of mineral alteration and weathering. Canadian Mineralogist, Special Publication 3, pp. 1–456.

Diraison, M., Cobbold, P.R., Gapais, D., Rossello, E.A. & Le Corre, C., 2000. Cenozoic crustal thickening, wrenching and rifting in the foothills of the southermost Andes, *Tectonophysics,* **316,** 91–119.

Di Vincenzo, G. & Laurenzi, M.A., 1999. Argon geochronology of small samples using the argon laserprobe facility at the IGGI-CNR, *Plinius,* **22,** 152–153.

Féraud, G., Alric, V., Fornari, M., Bertrand, H. & Haller, M., 1999. $^{40}$Ar/$^{39}$Ar dating of the Jurassic volcanic province of Patagonia: migrating magmatism related to Gondwana break-up and subduction, *Earth planet. Sci. Lett.,* **172,** 83–96.

Feruglio, E., 1944. Estudios geológicos y glaciológicos en la región del lago Argentino (Patagonia), *Bol. Acad. Nac. Ciencias,* Cordoba, **37,** 1–208.

Feruglio, E., 1949. *Descripción geológica de la Patagonia I,* YPF, Buenos Aires.

Furque, G., 1973. Descripción Geológica de la Hoja 58b, Lago Argentino, *Serv. Nac. Min. Geol.,* Buenos Aires, Bol. **140,** 1–51.

Geuna, S.E., Somoza, R., Vizán, H., Figari, E.G. & Rinaldi, C.A., 2000. Paleomagnetism of Jurassic and Cretaceous rocks in central Patagonia: a key to constrain the timing of rotations during the breakup of southwestern Gondwana?, *Earth planet. Sci. Lett.,* **181,** 145–160.

Giacosa, R.E., Franchi, M. & Genini, A., 1999. Hoja Geológica 4772-III Lago Belgrano, Hoja Geológica 4772-IV Lago Posadas, Provincia de Santa Cruz, *Serv. Geol. Min. Argent.,* Buenos Aires, Bol. **256**.

Gradstein, F.M., Agterberg, F.P., Ogg, J.G., Hardenbol, J., van Veen, P., Thierry, J. & Huang, Z., 1995. A Mesozoic time scale, *J. geophys. Res.,* **99,** 24 051–24 074.

Grunow, A.M., Dalziel, I.W.D., Harrison, T.M. & Heizler, M.T., 1992. Structural geology and geochronology of subduction complexes along the margin of Gondwanaland: new data from the Antarctic Peninsula and southernmost Andes, *Geol. Soc. Am. Bull.,* **104,** 1497–1514.

Grunow, A.M., Pankhurst, R.J., Rapela, C.W. & Marquez, M., 1993. Paleomagnetic and geochronologic results from lower Jurassic rocks in Southeastern Patagonia, Argentina, *EOS, Trans. Am. geophys. Un.,* 1993 Fall Meeting, 214.

Gust, D.A., Biddle, K.T., Phelps, D.W. & Uliana, M.A., 1985. Associated Middle to Late Jurassic volcanism and extension in southern South America, *Tectonophysics,* **116,** 223–253.

Haggerty, S.E., 1976. Oxidation of opaque mineral oxides in basalts, *Reviews in Min.,* **3,** Hg101–Hg300.

Haggerty, S.E., 1981. Oxide textures–a mini atlas, *Reviews in Min.,* **25,** 129–137.

Haggerty, S.E. & Lindsley, D.H., 1970. Stability of the pseudobrookite ($Fe_2TiO_5$)-ferropseudobrookite ($FeTi_2O_5$) series, *Carnegie Inst. Washington Year Book,* **68,** 247–249.

Halpern, M., 1973. Regional geochronology of Chile south of 50 latitude, *Geol. Soc. Am. Bull.,* **84,** 2407–2422.

Iglesia Llanos, M.P., 1997. Magnetoestratigrafia y paleomagnetismo del Jurásico inferior marino de la Cuenca Neuquina, República Argentina, *PhD thesis,* University of Buenos Aires, p. 337.

Iglesia Llanos, M.P. & Riccardi, A.C., 2000. The Neuquén composite section: magnetostratigraphy and biostratigraphy of the marine lower Jurassic from the Neuquén basin (Argentina), *Earth planet. Sci. Lett.,* **181,** 443–457.

Kay, S.M., Gorring, M.L. & Ramos, A.V., 1994. Magmas de arco, retroarco y fundidos de corteza oceánica asociados con la colisión de dorsales oceánicas en Patagonia, *7° Cong. Geol. Chileno,* Actas **2,** 1100–1104.

Kirschvink, J.L., 1980. The least-squares line and plane and the analysis of palaeomagnetic data, *Geophys. J. R. astr. Soc.,* **62,** 699–718.

Kraemer, P.E., 1993. Perfil estructural de la cordillera Patagónica Austral a los 50°S Santa Cruz, *13° Cong. Geol. Argent. y 2° Cong. Explor. de Hidrocarb.,* Actas **3,** 119–125.

Kraemer, P.E., 1994. Segmentación geológica y geofisica en la cordillera patagónica austral. Consecuencia de discontinuitades en el rift jurásico? 49°S–51°S Argentina y Chile, *7° Cong. Geol. Chileno,* Actas **1,** 71–75.

Kraemer, P.E., 1998. Structure of the Patagonia Andes: regional balanced cross section at 50°S, Argentina, *Int. Geol. Rev.,* **40,** 896–915.

Kraemer, P.E. & Riccardi, A.C., 1997. Estratigrafía de la región comprendida entre los lagos Argentino y Viedma (49°40′–50°10′ lat. S), Provincia de Santa Cruz, *Rev. Asoc. Geol. Argent.,* **52,** 333–360.

Kraemer, P.E., Ploszkiewicz, J.V. & Ramos, V.A., 2002. Estructura de la Cordillera Patagónica austral entre los 46° y 52°S, in *Geología y Recursos Naturales de Santa Cruz, Vols 1–22,* pp. 353–364, ed. Haller, M.J., *Relat. 15° Congr. Geol. Argent*.

Lema, H., Busteros, A. & Franchi, M., 2001. Hoja Geológica 4466 II y IV Camarones, Provincia del Chubut, *Serv. Geol. Min. Argent*., Buenos Aires, Bol. **261,** 1–60.

Lowrie, W., 1990. Identification of ferromagnetic minerals in a rock by coercivity and unblocking properties, *Geophys. Res. Lett.,* **17,** 159–162.

Massabie, A.C., 1990. La faja de corrimientos Río Turbio–La Leona y estructuras menores asociadas. Valle del río Leona, Santa Cruz, *Rev. Asoc. Geol. Argent.,* **45,** 29–36.

McArthur, A.N., Cas, R.A.F. & Orton, G.J., 1998. Distribution and significance of crystalline, perlitic and vescicular textures in the Ordovician Garth Tuff (Wales), *Bull. Volcanol.,* **60,** 260–285.

McClelland, E. & McCaig, A.M., 1989. Palaeomagnetic estimates of rotations in compressional regimes and potential discrimination between thin-skinned and deep crustal deformation, in *Paleomagnetic Rotations and Continental Deformation,* pp. 365–379, eds Kissel, C. & Laj, C., Kluwer Academic Publishers.

McFadden, P.L., 1990. A new fold test for palaeomagnetic studies, *Geophys. J. Int.,* **103,** 163–169.

McFadden, P.L. & McElhinny, M.W., 1988. The combined analysis of remagnetization circles and direct observations in palaeomagnetism, *Earth Planet. Sci. Lett.,* **87,** 161–172.

McFadden, P.L. & McElhinny, M.W., 1990. Classification of the reversal test in palaeomagnetism, *Geophys. J. Int.,* **103,** 725–729.

Mullender, T.A.T., van Velzen, A.J. & Dekkers, M.J., 1993. Continuous drift correction and separate identification of ferrimagnetic and paramagnetic contributions in thermomagnetic runs, *Geophys. J. Int.,* **114,** 663–672.

Nullo, F., 1978. Descripción geológica de la Hoja 56a-b, Cerro Fitz Roy (1:200.000), *Serv. Geol. Min. Argent.,* Buenos Aires, unpublished.

Nullo, F.E., Proserpio, C. & Ramos, V.A., 1978. Estratigrafía y tectónica de la vertiente este del Hielo Continental Patagónico, Argentina-Chile, *7° Congr. Geol. Argent.,* Actas **I,** 455–470.

Ogg, J.G., 1995. Magnetic polarity time scale for the Phanerozoic, *Global Earth Physics, A Handbook of Physical constants,* AGU, Washington, 240–270.

Oldow, J.S., Channell, J.E.T., Catalano, R. & D'Argenio, B., 1990. Contemporaneous thrusting and large-scale rotations in the Western Sicilian fold and thrust belt, *Tectonics,* **9,** 661–681.

Oviedo, E. & Vilas, J.F., 1984. Movimientos recurrentes en el Permo-Triásico entre el Gondwana Occidental y el Oriental, *9° Cong. Geol. Argent.,* Actas **3,** 97–114.

Pankhurst, R.J., Sruoga, P. & Rapela, C.W., 1993. Estudio geocronológico Rb-Sr de los complejos Chon-Aike y El Quemado a los 47°30′ L.S, *12° Cong. Geol. Argent.,* 171–178.

Pankhurst, R.J., Leat, P.T., Sruoga, P., Rapela, C.W., Marquez, M., Storey, B.C. & Riley, T.R., 1998. The Chon Aike province of Patagonia and related rocks in West Antarctica: A silicic large igneous province, *J. Volc. Geotherm. Res.,* **81,** 113–136.

Pankhurst, R.J., Riley, T.R., Fanning, C.M., Kelley, S.P., 2000. Episodic silicic volcanism in Patagonia and the Antarctic Peninsula: chronology of magmatism associated with the break-up of Gondwana, *J. Petrol.,* **41,** 605–625.

Panza, J.L. & Haller, M.J., 2002. El Volcanismo Jurásico, in *Geología y Recursos Naturales de Santa Cruz,* Vols 1–7, pp. 89–101, ed. Haller, M.J., *Relat. 15° Congr. Geol. Argent*.

Ramos, V.A., 1979. Tectónica de la región del Río y Lago Belgrano, Cordillera Patagónica–Argentina, *2° Cong. Geol. Chil.,* Actas, **1,** B2–B32.

Ramos, V.A., 1981. Descripción geológica de la Hoja 55a, Sierra de Sangra, Provincia de Santa Cruz (1:200.000), *Serv. Geol. Min. Argent.,* Buenos Aires, unpublished.

Ramos, V.A., 1982. Descripción geológica de las Hojas 53a–Monte San Lorenzo y 53b–Monte Belgrano, Provincia de Santa Cruz (1:200.000)., *Serv. Geol. Min. Argent.,* Buenos Aires, unpublished.

Ramos, V.A., 1983. Evolución tectónica y metalogénesis de la Cordillera Patagónica, *2° Congr. Nac. Geol. Econom.,* Actas **1,** 108–124.

Ramos, V.A., 1988. La estructura de la Cordillera Patagónica (47° –49° S) de Argentina y Chile, *5° Cong. Geol. Chileno,* Actas **1,** A101–A114.

Ramos, V.A., 1989. Andean foothills structures in northern Magallanes basin, Argentina, *Am. Ass. Petrol. Geol. Bull.,* **73,** 887–903.

Ramos, V.A., 2002. Evolución Tectónica, in *Geología y Recursos Naturales de Santa Cruz,* Vols 1–23, pp. 365–387, ed. Haller, M.J., *Relat, 15° Congr. Geol. Argent*.

Ramos, V.A., Niemeyer, H., Skarmeta, J. & Muñoz, M., 1982. Magmatic evolution of the Austral Patagonian Andes, *Earth Sci. Rev.,* **18,** 411–443.

Rapalini, A.E. & López de Luchi, M., 2000. Palaeomagnetism and magnetic fabric of Middle Jurassic dykes from Western Patagonia, Argentina. *Phys. Earth planet. Inter.,* **120,** 11–27.

Rapela, C.W. & Pankhurst, R.J., 1992. The granites of northen Patagonia and the Gastre Fault System in relation to the break-up of Gondwana, in *Magmatism and the Causes of Continental Break-up,* Vol. 68, pp. 209–220, eds Storey, B.C., Alabaster, T. & Pankhurst, R.J., *Geol. Soc. Spec. Publ.*

Rapela, C.W. & Pankhurst, R.J., 1993. El volcanismo riolítico del noreste de la Patagonia: un evento meso-jurásico de corta duración y origen profundo, *12° Cong. Geol. Argent.,* Actas **4,** 179–188.

Rapela, C.W. & Pankhurst, R.J., 1994. Variaciones temporales del magmatismo Jurásico de la Patagonia, *7° Cong. Geol. Chileno,* Actas **2,** 1433–1437.

Riccardi, A.C., 1971. Estratigrafía en el oriente de la Bahía de La Lancha, lago San Martín, Santa Cruz, Argentina, *Rev. Museo La Plata,* **7,** Geol. 61, 245–318.

Riccardi, A.C. & Rolleri, E.O., 1980. Cordillera Patagónica Austral, in *Segundo Simposio de Geología Regional Argentina,* Vol. 2, pp. 1173–1304, ed. Turner, J.C., Acad. Nac. de Ciencias, Córdoba.

Riccardi, A.C., Gulisano, C.A., Mojica, J., Palacios, O., Schubert, C. & Thomson, M.R.A., 1992. Western South America and Antartcica, in *The Jurassic of the Circum-Pacific,* pp. 122–161, ed. Westermann, G.E.G., Cambridge University Press.

Riggi, J.C., 1957. Resumen geológico de la zona de los lagos Pueyrredón y Posadas, provincia de Santa Cruz, *Rev. Asoc. Geol. Argent.,* **12,** 65–97.

Roperch, C., Chauvin, A., Calza, F., Palacios, C., Parraguez, G., Pinto, L. & Goguitchaivilli, A., 1997. Paleomagnetismo de las rocas volcánicas del Jurasico tardío al Terciario temprano de la región de Aysén (Coyhaique-Cochrane), *8° Cong. Geol. Chileno,* Actas **1,** 236–240.

Samson, S.D. & Alexander, E.C., Jr, 1987. Calibration of interlaboratory $^{40}$Ar-$^{39}$Ar dating standard, MMhb-1, *Chem Geol.,* **66,** 27–34.

Schmidt, V., 1990. Circularity of paleomagnetic data sets: An aid in the recognition of contaminating secondary overprints, *Tectonophysics,* **184,** 11–20.

Schwartz, S. & Van der Voo, R., 1984. Palaeomagnetic study of thrust sheet rotation during foreland impingement in the Wyoming-Idaho overthrust belt, *J. geophys. Res.,* **89,** 10 077–10 086.

Sruoga, P., 1989. Estudio petrológico del plateau ignimbrítico jurásico a los 47°30′ lat. S, *PhD thesis,* Universidad Nacional de La Plata.

Streck, M.J. & Grunder, A.L., 1995. Crystallisation and welding variations in a widespread ignimbrite sheet: the Rattlesnake Tuff, eastern Oregin, USA, *Bull. Volcanol.,* **57,** 151–169.

Suárez, M. & De la Cruz, R., 1997. Edades K-Ar del Grupo Ibañez en 2, 1433–1437.la parte oriental del Lago General Carrera (46°–47° L.S.) Aysén, Chile, *8° Cong. Geol. Chileno,* Actas, **2,** 1548–1551.

Suárez, M., Márquez, M. & De la Cruz, R., 1997. Nuevas edades K-Ar del Complejo El Quemado a los 47°13′–47°22′ L.S, *8° Cong. Geol. Chileno,* Actas, **2,** 1552–1555.

Valencio, D.A. & Vilas, J.F., 1970. Palaeomagnetism of some Middle Jurassic lavas from south-east Argentina, *Nature,* **225,** 262–264.

Valencio, D.A., Vilas, J.F. & Pacca, I.G., 1983. The significance of the paleomagnetism of the Jurassic-Cretaceous rocks from South America: predrift movements, hair-pins and magnetostratigraphy, *Geophys. J. R. astr. Soc.,* **73,** 135–151.

Vilas, J.F., 1974. Palaeomagnetism of some igneous rocks of the Middle Jurassic Chon-Aike Formation from Estancia La Reconquista, Province of Santa Cruz, Argentina, *Geophys. J. R. astr. Soc.,* **39,** 511–522.

Vizán, H., 1998. Paleomagnetism of the Lower Jurassic Lepá and Osta Arena formations, Argentine Patagonia, *J. S. Am. Earth Sci.,* **11,** 333–350.

Xu, W., Van der Voo, R., Peacor, D.R. & Beaubouef, R.T., 1997. Alteration and dissolution of fine-grained magnetite and its effects on magnetization of the ocean floor, *Earth planet. Sci. Lett.,* **151,** 279–288.

Zhou, W., Van der Voo, R., Peacor, D.R. & Zhang, Y., 2000. Variable Ti-content and grain size of titanmagnetite as a function of cooling rate in very young MORB, *Earth planet. Sci. Lett.,* **179,** 9–20.

Zijderveld, J.D.A., 1967. A.C. demagnetization of rocks, in *Methods in palaeomagnetism,* pp. 254–286, eds Collinson, D.W., Creer, K.M. & Runcorn, S.K., Elsevier, Amsterdam.

## APPENDIX A: $^{40}$Ar/$^{39}$Ar GEOCHRONOLOGY

The analysed sample, a polished section, was irradiated for 30 hr in the 1 MW TRIGA reactor (ENEA La Casaccia–Rome), using MMhb as flux monitor (520.4 ± 1.7 Ma; Samson & Alexander 1987). After the loading on an ultra-high vacuum extraction line, selected areas were fused using a focussed IR laser beam at the IGG-CNR laboratory in Pisa (see Di Vincenzo & Laurenzi 1999, for a description of the system). Owing to the low K contents of analysed minerals, 5–20 laser spot fusions (10–12 on average) on the selected area were used for each age datum, such that also the less gas-rich analysis had a signal/blank ratio of at least 10 (Table A1).

**Table A1.** $^{40}Ar/^{39}Ar$ laser spot fusions data, in ml STP. Reported errors are at the $1\sigma$ level and do not include uncertainty in the J value, which is only considered in the final age derived from the isochron plot. Symbols: fd = feldspar; gm = groundmass; b.d.l. = below detection limit.

| | $^{36}Ar_{atm}$ | $^{37}Ar_{Ca}$ | $^{38}Ar_{Cl}$ | $^{39}Ar_{K}$ | $^{40}Ar_{rad}$ | Age (Ma) | $\pm1\sigma$ | $^{40}Ar_{rad}$ (per cent) | K/Ca | $\pm1\sigma$ |
|---|---|---|---|---|---|---|---|---|---|---|
| fd | 6.329E-14 | 8.178E-12 | 4.250E-16 | 2.695E-12 | 3.178E-11 | 157.96 | 5.45 | 62.9 | 0.177 | 0.008 |
| fd | 1.823E-14 | 6.250E-12 | b.d.l. | 1.368E-12 | 1.530E-11 | 150.20 | 28.99 | 73.9 | 0.118 | 0.006 |
| fd | 1.828E-13 | 4.552E-11 | 7.643E-14 | 3.682E-12 | 3.277E-11 | 120.53 | 8.39 | 37.7 | 0.044 | 0.001 |
| fd | 1.584E-13 | 4.245E-11 | 4.250E-14 | 4.880E-12 | 4.520E-11 | 125.25 | 6.36 | 49.1 | 0.062 | 0.002 |
| fd | 6.184E-14 | 1.419E-11 | 2.394E-14 | 1.829E-12 | 2.214E-11 | 162.01 | 17.18 | 54.8 | 0.069 | 0.003 |
| fd | 7.328E-14 | 2.272E-11 | 6.398E-15 | 1.299E-11 | 1.511E-10 | 155.95 | 1.85 | 87.4 | 0.307 | 0.010 |
| fd | 7.085E-14 | 5.387E-12 | 3.587E-14 | 6.644E-13 | 4.463E-12 | 91.69 | 21.71 | 17.6 | 0.066 | 0.003 |
| fd | 6.603E-14 | 9.409E-12 | 7.255E-14 | 2.219E-12 | 2.333E-11 | 141.51 | 3.93 | 54.4 | 0.127 | 0.005 |
| fd | 1.405E-13 | 6.557E-13 | 9.059E-15 | 3.516E-12 | 3.931E-11 | 150.14 | 7.01 | 48.6 | 2.885 | 0.171 |
| fd | 1.327E-13 | 1.199E-12 | 2.955E-15 | 5.687E-12 | 5.608E-11 | 133.07 | 4.21 | 58.8 | 2.551 | 0.133 |
| fd | 1.219E-13 | 4.546E-13 | 5.927E-15 | 5.086E-12 | 5.332E-11 | 141.13 | 6.21 | 59.7 | 6.019 | 0.937 |
| fd | 5.723E-14 | 1.250E-12 | 1.613E-14 | 1.115E-12 | 1.191E-11 | 143.76 | 10.57 | 41.3 | 0.480 | 0.028 |
| gm | 2.958E-13 | 1.260E-12 | 7.561E-14 | 1.435E-11 | 1.324E-10 | 124.83 | 1.09 | 60.2 | 6.127 | 0.237 |
| gm | 4.460E-13 | 4.796E-12 | 3.769E-14 | 1.042E-11 | 9.399E-11 | 122.09 | 2.28 | 41.6 | 1.169 | 0.038 |
| fd | 7.843E-14 | 1.560E-11 | 6.149E-14 | 3.048E-12 | 3.238E-11 | 142.94 | 10.7 | 58.3 | 0.105 | 0.003 |
| fd | 4.563E-14 | 4.378E-12 | 1.357E-14 | 2.597E-12 | 2.935E-11 | 151.72 | 5.74 | 68.5 | 0.319 | 0.010 |
| fd | 6.180E-14 | 4.684E-12 | b.d.l. | 3.866E-12 | 4.156E-11 | 144.58 | 3.19 | 69.4 | 0.444 | 0.019 |
| fd | 6.957E-14 | 9.866E-12 | 1.274E-14 | 7.962E-12 | 9.264E-11 | 156.00 | 1.85 | 81.8 | 0.434 | 0.017 |
| fd | 4.878E-14 | 5.694E-12 | 8.254E-15 | 7.416E-12 | 8.355E-11 | 151.25 | 2.68 | 85.2 | 0.701 | 0.029 |
| fd | 5.313E-14 | 1.503E-12 | 9.063E-15 | 3.058E-12 | 3.313E-11 | 145.65 | 4.04 | 67.8 | 1.094 | 0.073 |
| fd | 6.963E-14 | 1.787E-12 | 4.104E-14 | 2.818E-11 | 2.610E-10 | 125.26 | 0.57 | 92.6 | 8.481 | 0.288 |
| fd | 4.072E-14 | 9.883E-13 | 8.787E-15 | 1.165E-11 | 1.089E-10 | 126.34 | 1.18 | 90.0 | 6.340 | 0.231 |
| fd | 2.407E-14 | 2.538E-12 | 6.704E-15 | 3.069E-12 | 3.481E-11 | 152.21 | 5.01 | 83.0 | 0.651 | 0.031 |
| fd | 6.171E-14 | 4.599E-12 | b.d.l. | 2.162E-12 | 1.826E-11 | 114.56 | 4.79 | 50.0 | 0.253 | 0.009 |
| fd | 1.205E-13 | 3.213E-12 | 5.656E-15 | 1.886E-11 | 2.267E-10 | 160.88 | 1.8 | 86.4 | 3.159 | 0.099 |
| fd | 6.151E-14 | 2.520E-12 | 1.615E-14 | 2.149E-12 | 2.176E-11 | 136.49 | 10.76 | 54.5 | 0.459 | 0.024 |

J = 0.007762 (±0.0000343)
$(^{39}Ar/^{37}Ar)_{Ca}$ = 0.000686 (±0.000034)
$(^{36}Ar/^{37}Ar)_{Ca}$ = 0.000288 (±0.000014)
$(^{40}Ar/^{39}Ar)_{K}$ = 0.00757 (±0.00038).